SEMI-ANNUAL STATUS REPORT

June 1972

SOLAR WIND PHYSICS

NASA Grant NGR 50-002-162

Department of Physics
University of Wisconsin
Madison, Wisconsin 53706

A. Solar Wind Composition

1. In order to develop an instrument which can determine the charges and masses of solar wind ions, we have constructed a double-chamber gas proportional counter to detect and identify solar wind ions after they have been accelerated by the high voltage power supply that we have developed and described in previous progress reports. An ion enters the front chamber of the proportional counter through a very thin Formvar window. The front chamber is made thin enough so that an ion traverses it without stopping and then enters the back chamber where it stops. The pulse from the front chamber and the pulse from the back chamber together give information about the total energy E of the ion which then determines the ion charge q since $E \simeq qV$, where V is the known accelerating voltage provided by the high-voltage power supply. Further, the pulse from the front chamber also can be used to determine the ion mass m since the energy loss in the front chamber depends on the ion's velocity v which in turn depends on the ion's mass for given charge q and accelerating voltage V.

A "breadboard" model of the double-chamber proportional counter was exposed to beams of light ions in order to partially simulate solar-wind conditions. Some of the pulse-height spectra obtained from the front chamber are illustrated in Figure 1. These spectra were obtained requiring the back chamber to give coincidence pulses but without further analysis of the back chamber pulses. It can be seen from Figure 1a that this early version of the proportional counter could easily separate $^4He^+$ from $^1H^+$ which is necessary if interstellar helium is to be detected using interplanetary spacecraft.

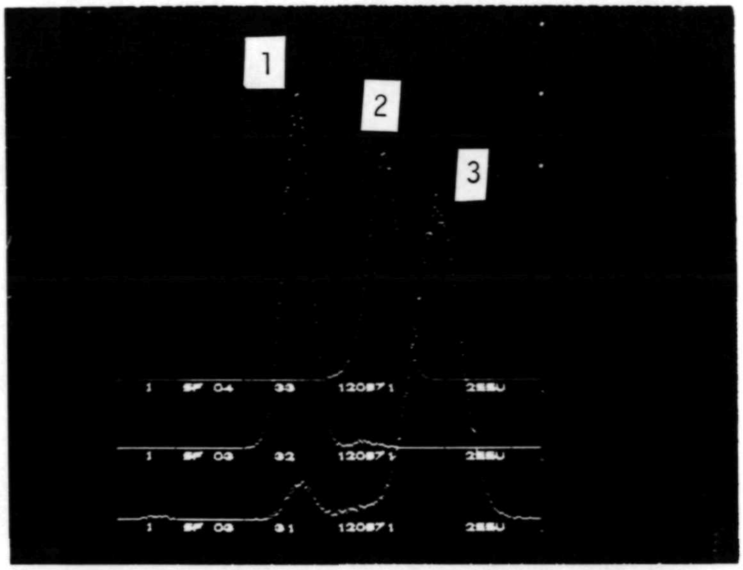

Figure 1a

1) 100 kev $^{4}He^{+}$

2) 100 kev $^{1}H^{+}$

3) 200 kev $^{4}He^{++}$

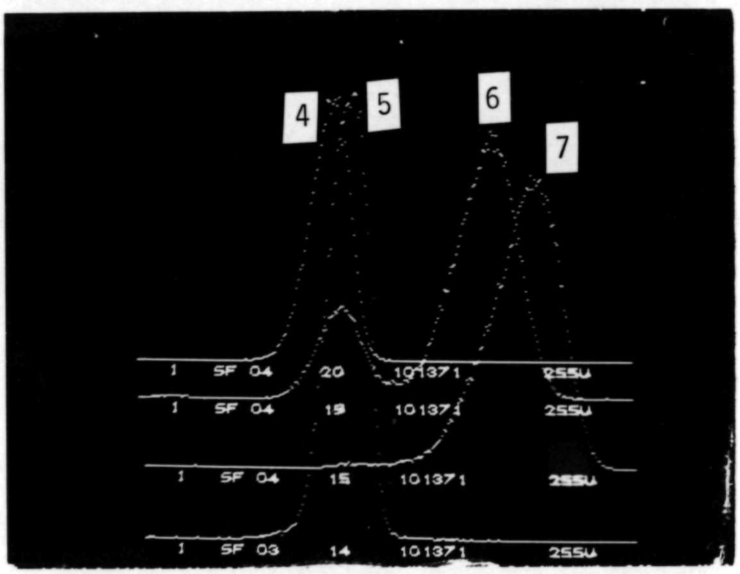

Figure 1b

4) 100 kev $^{4}He^{+}$

5) 100 kev $^{3}He^{+}$

6) 200 kev $^{4}He^{++}$

7) 200 kev $^{3}He^{++}$

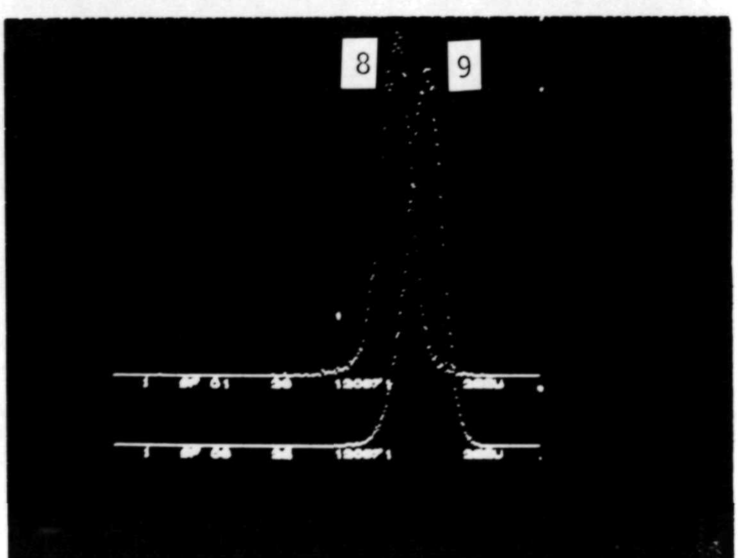

Figure 1c

8) 100 kev $^{2}D^{+}$

9) 100 kev $^{1}H^{+}$

Further, the front chamber clearly resolved $^{1}H^{+}$ and $^{4}He^{++}$ without additional spectral information from the back chamber which of course would have clearly distinguished between singly-charged hydrogen and doubly-charged helium. Figure 1b shows that $^{3}He^{++}$ and $^{4}He^{++}$ can be resolved but it may not be possible to resolve $^{4}He^{+}$ and $^{3}He^{+}$. Figure 1c shows that it would be difficult to resolve $^{2}D^{+}$ and $^{1}H^{+}$ if hydrogen were much more abundant than deuterium, as is expected. Thus the best method of detecting deuterium in the solar wind is to use a tritium target as originally proposed for IMP H and J.

We were encouraged by these results to build an improved proportional counter, which was recently completed, and to test it with moderately heavy elements such as ^{12}C, ^{16}O, ^{20}Ne, etc. Since our present laboratory source of ion beams can only produce singly-charged or doubly-charged ions, we cannot simulate highly stripped solar wind ions exactly. However, we will be able to produce ions of the correct energy by increasing the laboratory ion accelerator voltage to 300 kilovolts with a pelletron power supply purchased from National Electrostatics Corporation. Thus, for example, we will be able to produce beams of 600 kev $^{16}O^{++}$ which will simulate solar wind $^{16}O^{6+}$ ions accelerated across a 100 kilovolt gap in a spacecraft instrument before entering the proportional counter. The charge of the ion incident on the front window of the proportional counter doesn't really matter since the ion reaches charge exchange equilibrium in the Formvar window before it enters the front chamber.

2. Following a suggestion made to us by Dr. L. Kavanagh of NASA head-

quarters, we are proceeding with plans to measure the charges and masses of positive ions in a hydrogen aurora using the techniques we have developed for solar wind ions. Recent sounding rocket observations of ions in auroras (Whalen et al., 1971; Whalen and McDiarmid, 1972) have detected H^+ and He^{++} ions above the atmosphere in the 2 to 20 kev energy range, whereas no He^+ ions were observed. These results were interpreted as suggesting that the auroral ions originated in the solar wind and were injected into the magnetosphere with approximately the same probability per ion incident on the magnetosphere. If the solar wind is in fact the source of auroral ions then it should be possible at sufficiently high altitudes, to detect not only H^+ and He^{++} ions in an aurora, but also O^{6+}, O^{7+}, and other heavy ions which are known to be present in the solar wind. On the other hand, if auroral H^+ and He^{++} ions originate in the magnetosphere, then there should be no highly charged heavier ions in auroras. It is important to stress that such observations must be carried out at altitudes above about 400 kilometers so that the heavy ions will not charge-exchange with residual atmospheric gases. Thus the only sounding rocket suitable for such an experiment is the Javelin.

We have visited the GSFC sounding rocket division for preliminary discussions to formulate a specific design of an experiment to be launched on a Javelin vehicle from Fort Churchill. A proposal for this experiment is now being prepared and will soon be submitted to NASA.

F. Scherb
J. Lynch
K. Walker
J. Peters

B. Interstellar Gas in Interplanetary Space

1. As members of the plasma team for the mission definition phase of the Outer Planets Missions, we have analyzed in detail the feasibility of detecting H^+ and He^+ ions of interstellar origin. The results of our calculations have been summarized in the Plasma Team Midterm Report, dated February 1, 1972, and a copy of our summary is included in this report as Appendix A. In addition, a detailed analysis of the He^+ velocity distribution at 1 AU will be published in the Journal of Geophysical Research; a copy of the paper is given in Appendix B of this report.

2. A program to carry out ground-based astronomical observations of faint, diffuse optical emission lines from interstellar gas has been operating successfully at the GSFC 36-inch telescope during the past eight months. We have detected faint hydrogen and oxygen emission lines from galactic sources and we have clearly resolved galactic and geocoronal $H\alpha$ and $H\beta$ emission lines. The high-resolution 150 mm Fabry-Perot scanning spectrometer being used for these observations is a superb instrument. We believe that the results obtained so far are very useful for analyzing the mechanisms which ionize and heat the interstellar medium. Furthermore, we have discovered a geocoronal night-sky $H\beta$ emission line which is not explained by existing models of night-sky geocoronal hydrogen Balmer emission lines. The results of these observations will be submitted soon for publication in the Astrophysical Journal. A copy of this paper is presented in Appendix C.

   This program is a collaboration between the University of Wisconsin and Goddard Space Flight Center. Dr. R. Reynolds is presently at GSFC as a NAS-NRC postdoctoral associate. F. Scherb will join him in September, 1972, for one year as a NAS-NRC senior postdoctoral associate at GSFC to carry out observations of galactic emissions, interplanetary emission lines, and geocoronal emissions. Professor F. Roesler will provide additional program direction and support at the University of Wisconsin. We also expect to work closely with Dr. Elihu Boldt of GSFC.

F. Scherb
D. Goldstein

References

Whalen, B. A., J. R. Miller, and I. B. McDiarmid, "Evidence For a Solar Wind Origin of Auroral Ions From Low-Energy Ion Measurements", J. Geophys. Res., 76, 2406, 1971.

Whalen, B. A. and I. B. McDiarmid, "Further Low-Energy Auroral Ion Composition Measurements", J. Geophys. Res., 77, 1306, 1972.

Papers and Talks

W. C. Feldman, D. Goldstein and F. Scherb, "Annual Variation of the Interplanetary He^{+} Velocity Distribution at 1 AU", to be published in the Journal of Geophysical Research.

R. J. Reynolds, F. L. Roesler and F. Scherb, "Low Intensity Balmer Emissions from the Interstellar Medium and Geocorona", to be submitted to the Astrophysical Journal.

R. J. Reynolds, F. L. Roesler, and F. Scherb, "Local and Galactic Contributions to the Hα and Hβ Night Sky Emission Lines", paper presented at the 53rd Annual Meeting of the AGU, Washington, D. C., April, 1972.

Staff

F. Scherb	Professor
J. Lynch	Research Associate
H. Christianson	Technician
K. Walker	Technician (Space Science & Engineering Ctr)
K. Brager	Secretary

Detection of Ionized Interstellar Gas and Solar Wind Ions Neutralized by Interplanetary Dust Grains

F. Scherb and W. C. Feldman*
Department of Physics, University of Wisconsin

Missions to the outer planets provide an ideal opportunity to study solar wind ions in interplanetary space. Measurable fluxes of such ions are expected to originate from neutral gas clouds of interstellar origin in interplanetary space and maybe from the outgassing of planetary satellites, asteroidal bodies and interplanetary dust grains.

Lyman alpha observations carried out by instruments on OGO 5, Vela 7, Mariners 5 and 6, and other spacecraft provide strong evidence that neutral atomic hydrogen is present in interplanetary space. A plausible source for this hydrogen is the interstellar medium in which the solar system is immersed. However, if neutral interstellar gas is to penetrate into the solar system to distances within a few astronomical units (AU) of the sun, it is necessary to assume that the interstellar gas has a macroscopic velocity relative to the sun, i.e., we must have an "interstellar wind."

In addition to hydrogen, other normally neutral constituents of the interstellar medium would be present in interplanetary space. For example, helium is a likely possibility.

Atoms of the interstellar wind that are ionized in interplanetary space by solar EUV or by the solar wind are mostly swept away from the sun by macroscopic interplanetary electromagnetic fields associated with the solar wind (and, to some extent, by interactions with the microscale structure of the fields). The two most suitable candidates for detection and identification are H^+, He^+. These species would be readily distinguishable from solar wind ions by their anomalous velocity distributions and by the fact that their flux densities will exhibit heliocentric radial dependences which differ from the r^{-2} dependence of the solar wind flux density. Observations of interstellar wind ions may be useful in determining the density, composition, and temperature of the local interstellar medium.

We can estimate the counting rate of H^+ and He^+ ions of interstellar origin expected for an instrument similar in design to a LEPEDEA with cylindrical analyzer central angle $\phi_o = 45°$, $\Delta r_o = .7$ cm, $r_o = 13.15$ cm and effective collecting area $A = .6\ cm^2$. We chose the model of the local interstellar medium proposed to explain the OGO 5 Lyman alpha observations. Here $n_H(r = \infty) = .1\ cm^3$, $n_{He}(r = \infty) = .005\ cm^{-3}$, $< \bar{V} >_{r=\infty} = 10$ km/sec and $T_{(r=\infty)} = 100$ °K and 5000 °K. For this calculation we neglect the effect of magnetic irregularities convected by the solar wind on the acceleration of interstellar H^+ and He^+ injected into the solar wind. Equivalently we assume a minimum scattering length, $\lambda(r)$ with respect to convected magnetic irregularities. Thus, for regions of interplanetary space sampled, Δr, corresponding to a velocity measurement interval Δv, $\Delta r < \lambda(r)$. Furthermore, for interstellar hydrogen we assume the Ly-α pressure balances the solar gravitational force. Below we tabulate the expected counting rate at the high velocity cutoff of the expected flux distribution as a function of r for H^+ and He^+ ions (He^+ ions will contribute two separate velocity distributions corresponding to clockwise and counterclockwise neutral He orbits about the sun) for both T = 100° and 5000° and $< \bar{V} >$ oriented in the ecliptic. The expected background counting rate is _______.

*Presently at Los Alamos Scientific Laboratory, Los Alamos, New Mexico

Furthermore, outer planet missions provide a unique opportunity to detect and identify atomic and molecular ions which escape from solar system bodies. Such ions are swept away by interplanetary electromagnetic fields and can readily be distinguished from solar wind ions by their anomalous velocity distribution, mass/charge ratios, and heliocentric radial gradients of their flux densities.

Expected LEPEDEA Counting Rate in Counts/Sec

Spacecraft Position		H			He				
					Clockwise		Counterclockwise		
Ecliptic Longitude with Respect to Apex	Helio-centric Radius	T = 100	T = 5000	λ(r) in AU	T = 100°	T = 5000°	T = 100°	T = 5000°	λ(r) in AU
180°	1	0	.2	.02	575	81	490	34	.12
210°	3	.02	12.7	.09	15	18	8	8.5	.2
250°	5	26	52	.16	3.2	4	3	3.5	.35
270°	7	51	64	.24					
270°	10	57	64	.35	1.3	1.8	1.3	1.6	.5

APPENDIX B

Annual Variation of the Interplanetary He^+ Velocity Distribution at 1 AU

W. C. Feldman,* D. Goldstein, and F. Scherb

University of Wisconsin, Madison, Wisconsin 53706

Abstract

The interplanetary velocity distribution of He^+ ions of interstellar origin is calculated for various ecliptic longitudes Φ, at 1 AU and for various temperatures, T, of the local interstellar medium. For concreteness we assume a relative streaming velocity of the local interstellar medium with respect to the sun of $\langle \bar{V}_\infty \rangle$ = 10 km/sec oriented in the ecliptic plane, $n_{He}(r = \infty) = 0.005\ cm^{-3}$ and we neglect interaction with magnetic irregularities convected by the solar wind. We find that these He^+ fluxes should be observable at 1 AU with present observation techniques and that if $T \simeq 100$ K they should exhibit sharp peaks which vary systematically with Φ. If $T \simeq 5000$ K, He^+ fluxes should appear almost structureless except for a well-defined high-energy cutoff. The annual variation of He^+ flux at this cutoff should exhibit a peak in the anti-apex direction with peak-to-valley ratio of 6:1 and $\Delta\Phi_{FWHM} = 70°$ for T = 5000 °K.

*Now at University of California, Los Alamos Scientific Laboratory, Los Alamos, New Mexico 87544

Introduction

Recent observations of Lyman α sky-background radiation by Thomas and Krassa [1971] and Bertaux and Blamont [1971] provide strong evidence for neutral hydrogen in interplanetary space. Thomas [1971] has presented an analysis of the observations in which these atoms are assumed to be a neutral component of the local interstellar medium interpenetrating and flowing through interplanetary space. An excellent review of the subject up to the beginning of 1971 is given by Axford [1971].

It has been pointed out (see e.g., Axford [1971] and references therein; Feldman et al. [1971]) that one should also expect neutral He atoms in interplanetary space. The initially freely streaming He atoms are gravitationally focused by the sun. A fraction is photoionized and subsequently caught up by the solar wind to be transported out of the solar system. It is of interest to consider (1) whether these He^+ particles are observable at 1 AU; (2) if they are observable, what is the nature of the velocity distribution function at r = 1 AU; and (3) what can be learned about the parameters of the local interstellar medium if the He^+ flux can be separated from the solar wind which is many orders of magnitude more intense.

In this paper we attempt to answer the above questions by calculating the velocity distribution function of He^+ particles of interstellar origin at 1 AU for various ecliptic longitudes. We assume a solar wind velocity V_{SW} = 400 km/sec, a solar velocity relative to the local interstellar medium $<\vec{V}_\infty>$ = 10 km/sec oriented in the ecliptic [Thomas 1971], a neutral He number density far from the sun, $n_{He}(\infty) = 0.005\ cm^{-3}$ and various temperatures of the local interstellar medium. Since existing data from a number of hemispherical electrostatic analyzers may be relevant to these calculations we apply the calculated flux distribution to obtain the peak counting rate expected for a plasma probe similar in design to the Vela 5 and 6 heavy ion detectors. In particular, whenever reference is made to expected instrumental response in this paper we choose the relevant acceptance characteristics of the above instruments which are: $\Delta V/V = 0.0195$, aperture area = 0.14 cm^2 and energy bin sample time τ = 112 msec which corresponds to a $(\Delta V/V) = 0.176$ sampling interval. Here ΔV and V are the velocity width and nominal acceptance velocity of the analyzer, respectively, for a given voltage applied to the hemispherical plates.

2. Interaction with Magnetic Irregularities Convected by the Solar Wind

In order to predict charged particle spectra to be observed at 1 AU due to He^+ particles of interstellar origin, two alternative assumptions have been made [Holzer and Axford, 1971, and Feldman et al., 1971] concerning the interaction of a test particle with the solar wind. Holzer and Axford [1971] have assumed a very strong interaction with magnetic irregularities convected by the solar wind so that a test particle would very quickly acquire solar wind bulk speed. On the other hand, Feldman, Lange, and Scherb [1971] have computed He^+ particle trajectories assuming a quiet solar wind with an Archimedean spiraled, noise-free magnetic field imbedded in the plasma. The actual interaction lies somewhere between these two extremes. Unfortunately, it is difficult to calculate the scattering length of a low-energy particle injected into the solar wind since there is no agreement yet as to the nature of the observed high frequency interplanetary magnetic field fluctuations. A rough estimate of the interaction time [Feldman et al., 1971], assuming the observed fluctuations at 1 AU during quiet times are not convected tangential or contact discontinuities, yields a scattering length of about 0.5 AU. Although this value is very uncertain, we feel it provides sufficient justification to assume a perfectly quiet magnetic field in this analysis of expected He^+ fluxes at 1 AU.

3. The He^+ Velocity Distribution for a Cold Interstellar Medium

The orbits of He^+ particles of interstellar origin injected into the solar wind have been calculated by Feldman et al. [1971] for various $<\vec{V}_\infty>$. We first briefly summarize their results and then select $<\vec{V}_\infty> = 10$ km/sec oriented in the ecliptic, with observation position of the He^+ particles situated in the ecliptic plane.

The coordinate system relevant to the interstellar infall problem is shown in Figure 1. The sun is assumed to have a velocity $- <\vec{V}_\infty>$ relative to a cold ($T \sim 100$ K) interstellar medium such that in the frame of reference with the sun at rest at the origin, neutral He atoms are streaming parallel to the X-Z plane at an angle Θ with respect to the Z axis. (All numerical results in this paper are for $\Theta = 90°$.) The positive Z axis is oriented northward perpendicular to the ecliptic; the X-Y plane is coincident with the ecliptic. Infalling He atoms follow hyperbolic trajectories before being ionized by solar EUV. Each He atom hyperbolic orbit is planar. Every point in the orbit plane can be specified equivalently by the heliocentric radial distance r_o and the angle δ_o between $\vec{r}_o$ and $<\vec{V}_\infty>$, or by two impact parameters p_1 and p_2 identifying a counterclockwise orbit and a clockwise orbit (when viewed from the north) respectively, which both pass through that point. After ionization, the He^+ particles are accelerated by a radially convected spiral magnetic field. Although the spiral magnetic field pattern is cylindrically symmetric, the subsequent He^+ trajectories are not so, due to the asymmetric initial injection velocities. For a cold interstellar medium the initial injection velocities are calculated assuming all He atoms travel with velocity $<\vec{V}_\infty>$ at large r.

The motion of a test particle in the radially convected interplanetary magnetic field can be separated into three components: (1) The superposition $\vec{V}_D$ of various drift velocities perpendicular to the magnetic field $\vec{B}$, (2) A circulating velocity $\vec{V}_\perp$ about the direction of the magnetic field, and (3) A velocity $\vec{V}_{\parallel}$ parallel to the magnetic field direction.

To a good approximation $V_D = V_{sw} \sin \chi$ with direction perpendicular to $\vec{B}$ but confined to the cone specified by polar angle $\theta = \theta_o$ where V_{sw} equals the constant solar wind speed, χ = the angle of $\vec{B}$ with respect to $\vec{r}$, and θ_o = the polar angle at injection. Thus to observe He^+ particles in the ecliptic, they must have been injected in the ecliptic.*

In the adiabatic limit $V_\perp$ is determined by the conservation of the magnetic moment μ given by

$$\mu = \frac{mV_\perp^2}{2B} \quad .$$

The equation governing the motion parallel to the field direction can be integrated exactly to obtain an analytic expression for $V_{\parallel}(r)$ which is a function of azimuthal injection position Φ_o, as well as heliocentric injection radius r_o. Thus if r_o, Θ_o, Φ_o are specified, the total noncirculating velocity is given by $\vec{V} = \vec{V}_{\parallel} + \vec{V}_D$. The equation for the orbit can then be written as

$$\frac{dr}{d\Phi} = \frac{r \sin \theta \; V_r}{V_\Phi}$$

*A brief remark on our notation is in order. We use (r_o, Θ_o, Φ_o) to specify the coordinates where ionization of a neutral He atom occurs whereas (r, Θ, Φ) denote the coordinates of the observer detecting the He^+ particles. In general, a subscript zero refers to injection into the solar wind.

where $V_r = V_{\parallel} \cos \chi + V_{sw} \sin^2 \chi$

and $V_\Phi = -V_{\parallel} \sin \chi + V_{sw} \sin \chi \cos \chi$

with $$\chi(r) = \cos^{-1}\left\{\left[1+\left(\frac{rw \sin \theta}{V_{sw}}\right)^2\right]^{-1/2}\right\}$$

and w = the angular speed of rotation of the sun.

The orbital equation was integrated numerically (for a specified $\langle\vec{V}_\infty\rangle$) to obtain a family of orbits as a function of (r_o, Φ_o). Thus a function $\Phi(r, r_o, \Phi_o)$ was obtained. After inverting $\Phi(r, r_o, \Phi_o)$ to obtain $\Phi_o(r, r_o, \Phi)$, the velocity distribution function of He^+ particles at (r, Φ) was synthesized by summing the contributions from each (r_o, Φ_o).

It was found that the region in velocity space occupied by these He^+ particles at 1 AU depends only weakly on Φ and $\langle\vec{V}_\infty\rangle$. Thus a representation of the phase space volume occupied for one particular (r, Φ) and $\langle\vec{V}_\infty\rangle$ will adequately characterize the ensemble of possible volumes. The projection onto the ecliptic of the region of occupation in velocity space is drawn in Figure 2 for a cold interstellar medium with $\langle\vec{V}_\infty\rangle$ = 10 km/sec, r = 1 AU and $\Phi = 190°$. Since the orbits of test particles injected into the solar wind are helices the actual velocity distribution consists of a sequence of circles with centers ordered along the magnetic field direction according to r_o. Since μ is constant, the circles occupied by He atoms ionized at smaller r_o will be smaller than those ionized at larger r_o. Both the location of the centers of the circles as well as the radii of the circles depend upon the initial conditions which are different for counterclockwise and clockwise neutral He orbits about the sun. Thus, if interaction with magnetic irregularities can be ignored the velocity distribution function expected at 1 AU consists of two sequences of circles, each circle corresponding to some r_o.

In Figure 2, the circle centered at longitudinal speed = 400 km/sec represents the projection of a spherical solar wind velocity distribution with 40 km/sec thermal speed. The shaded box represents the (projected) volume of velocity space that a hemispherical analyzer (similar to the Vela 5 and Vela 6 heavy ion detectors) would accept if its acceptance fan were oriented perpendicular to the ecliptic and at an angle ϕ with respect to the sun-vehicle direction. Another view looking along the magnetic field direction is shown in Figure 3. Assuming an instrumental resolution of $\Delta V/V = 0.0195$, the thickness of the spherical acceptance wedge in this case is 10 km/sec and about 1/10 of the velocity circle is accepted. Since the He^+ particles are uniformly distributed around the circle, about 1/10 of the particles injected at the corresponding r_o are accepted. For smaller analyzer acceptance speeds, the acceptance wedge intersects the same velocity circle along two short segments situated symmetrically with respect to the ecliptic plane. This results in a large reduction (by about a factor of 5) in the velocity space overlap between the instrument acceptance wedge and the He^+ particle population. Thus to a reasonable approximation, the observed He^+ velocity distribution function can be constructed by considering only the outer segments of each velocity circle drawn in Figure 2.

The He^+ flux corresponding to a given velocity circle segment is given by [Feldman et al., 1971]

$$F_V^{(J)} dV = F^{(J)}(V,\phi) \left(\frac{dr_o}{dV}\right) dV$$

$$F_\phi^{(J)} d\phi = F^{(J)}(V,\phi) \left(\frac{dr_o}{d\phi}\right) d\phi$$

where

$$F^{(J)}(V,\Phi) = \frac{n_{He}^{(J)}(r_o, \Phi_o)\ P(r)\ V^{(J)}(r,\Phi;\ r_o, \Phi_o)}{V_r^{(J)}(r, \Phi;\ r_o, \Phi_o)} \left(\frac{d\Phi_o}{d\Phi}\right)$$

Here J = 1 denotes a He orbit which does not circle behind the sun before ionization, and J = 2 corresponds to a He orbit which circles behind the sun before ionization. (See e.g., orbits labeled by p_1 and p_2, respectively, in Figure 1.) $P(r) = 6.8 \times 10^{-8}$ sec^{-1} is the probability per sec for ionization at r = 1 AU, $n_{He}^{(J)}(r_o, \Phi_o)$ is the neutral He number density at (r_o, Φ_o), (see e.g. equation 1 of Feldman, et al. 1971), $V^{(J)}(r, \Phi; r_o, \Phi_o)$ is the speed characterizing the outer segment of the velocity circle corresponding to (r_o, Φ_o), $V_r^{(J)}(r, \Phi; r_o, \Phi_o)$ is the radial velocity component of the He^+ particle center of gyration, $d\Phi_o/d\Phi$ accounts for the azimuthal focusing properties of the interplanetary medium and $F_V^{(J)}$ and $F_\phi^{(J)}$ denote the differential He^+ flux summed over all V and Φ, respectively.

As is well known (see e.g., Danby and Camm, 1957) the expression for $n_{He}^{(J)}(r_o, \Phi_c)$ is singular for $\Phi_o = 180°$ and T = 0 K. For T > 0 K the singularity disappears. Danby and Bray [1967] have calculated the density of interstellar matter near a star for T > 0 K neglecting ionization loss. Feldman, et al. [1971] included ionization loss of the neutral He to obtain an analytic expression for $n_{He}^{(J)}(r_o, 180°)$ which is valid for

$$\frac{m\langle V_\infty\rangle^2}{2kT} \gg 1,$$

where m is the atomic He mass. Their result is

$$n_{He}(r_o, 180°) = n_{He}(\infty)\left(\frac{\pi GM}{rkT}\right)^{1/2} \exp\left[\frac{-\pi r^2 P(r)}{(2GMr)^{1/2}}\right] \qquad (1)$$

where G is the gravitational constant, k is Boltzmann's constant, M is the solar mass, and $n_{He}(\infty)$ is the interstellar neutral He number density far from the sun.

Off-axis values of n_{He} (r_o, Φ_o) were generated using the parabolic interpolation formula

$$n_{He}(r_o, \Phi_o) = n_{He}(r_o, 180°)\ (1-D\delta^2) \tag{2}$$

where $\delta = \pi-\Phi_o$, and D is determined by fitting expression (2) onto the zero-temperature expression for $n_{He}(r_o, \Phi_c)$ at some angle $\Phi_c = \pi-\delta_c$. δ_c is determined by requiring a continuous first derivative at the interface of expression (2) with the zero-temperature expression for $n_{He}^{(J)}(r_o, 180-\delta)$ with $\delta \neq 0$.

For $\langle V_\infty \rangle$ = 10 km/sec,

$$\frac{m \langle V_\infty \rangle^2}{2kT} \geq 10 \text{ for } T \leq 2.4 \times 10^3 \text{ K.}$$

Thus expressions (1) and (2) above are certainly valid for T = 100 K. The angle-integrated fluxes of He^+ particles resulting from counterclockwise neutral He orbits are plotted in Figure 4 as a function of V for $\langle V_\infty \rangle$ = 10 km/sec oriented in the ecliptic plane, T = 100 K, $n_{He}(\infty)$ = 0.005 cm^{-3} (corresponding to a 5% He/H abundance and $n_H(\infty)$ = 0.1 cm^{-3}) and for various ecliptic observation longitudes. To simplify the calculation we have chosen a constant accepted circle segment length of 1/10 the full velocity circle. Thus the flux versus velocity curves in Figure 4 do not exactly correspond to actual measurements made with a hemispherical electrostatic analyzer. However, the discrepancy is not large because of competing effects: first, the He^+ particles originating at smaller r_o correspond to velocity circles with smaller radii. The geometry of the velocity space acceptance wedge of a hemispherical analyzer is such that a larger fraction of these particles are accepted. This effect is augmented by the fact that the smaller circles appear slightly flattened due to a projection effect thereby increasing the fraction of the He^+ population accepted. The summed instrumental enhancement of lower velocity fluxes with respect to the curves plotted in Figure 4 is roughly 50% for those velocities corresponding to an injection radius of 0.5 AU. The enhancement is larger for smaller r_o but for these He^+ particles we expect rather large modifications of the flux distribution due to interaction with convected magnetic irregularities. Second, the He^+ particles injected at smaller r_o correspond to lower V in Figure 4. Since $\Delta V/V$ = constant for a curved plate electrostatic analyzer, their counting rate is depressed relative to the He^+ particles injected at larger r_o. The magnitude of this effect is such as to nearly offset the previous enhancement. Thus the fluxes illustrated by Figure 4 represent a reasonable approximation to what actually would be observed under the above assumptions using a hemispherical electrostatic analyzer similar to the Vela 5 and 6 heavy ion detectors.

We note that the flux-versus-velocity curves plotted in Figure 4 exhibit narrow peaks which shift in velocity as Φ changes. These peaks result from the presence of a dense neutral He tail in the anti-apex direction. Note also that there is a marked variation in intensity with Φ as seen by comparing the curve for $\Phi = 90°$ with the curve for $\Phi = 180°$. The flux-versus-velocity curves for clockwise orbits shown in Figure 5 give qualitatively similar results. No curve is shown for $\Phi = 90°$ because for He^+ particles to be detected here, neutral He atoms would have to circle nearly all the way around the sun. The probability that this happens is small due to photoionization losses.

Figure 6 shows the velocity integrated He^+ fluxes F_ϕ as a function of ϕ for counterclockwise orbits, T = 100 K, $<V_\infty>$ = 10 km/sec and $n_{He}(\infty) = 0.005\ cm^{-3}$. Here too, sharp peaks are obtained which move toward smaller angles as the observer moves counterclockwise (increasing Φ) away from the anti-apex direction. Qualitatively similar results are obtained for clockwise orbits but are not shown. It should be noted that the curves in Figure 6 do not take into account instrumental broadening. Furthermore, the curves which peak in the range $\phi = 25°$ to 30° as well as the corresponding peaks in Figures 4 and 5 are composed of He^+ particles ionized at $r_o \leq 0.5$ AU. One might expect some modifications here due to pitch-angle scattering by convected magnetic irregularities.

4. The He^+ Velocity Distribution for a Warm Interstellar Medium

Even though in the previous section we used a non-zero temperature to calculate neutral He number densities in the high-density tail region, the He^+ orbits were computed using zero-temperature initial conditions. This is not strictly correct since a non-zero temperature of the interstellar medium translates into a velocity spread at all locations in the interplanetary medium. Since the He^+ orbits depend (weakly) on the initial velocity conditions, this leads to a spread in Φ at r = 1 AU for all those He atoms ionized at (r_o, Φ_o). Inverting the problem, an observer at (r, Φ) sees He^+ particles injected from a non-zero azimuthal neighborhood of Φ_o at r_o. The magnitude of this effect was investigated by calculating the He^+ orbits for various initial velocities $\vec{V}_\infty$ at $r = \infty$, corresponding to the spread expected for various T. It was found that the peaks plotted in Figures 4 through 6 would be broadened by less than 2% due to this effect. Of course the source region about (r_o, Φ_o) for detection at (r, Φ) enlarges with T. But for large T the neutral He high-density tail becomes diffuse so that here again the relative broadening of the velocity distribution function due to this effect is negligible. Thus, in our calculations of the velocity distribution function for arbitrary T we have assumed zero-temperature initial conditions for the He^+ orbits.

The dominant contribution to the change in character and intensity of the observed He^+ flux at 1 AU is due to the variation with T of the He atom density in the high-density tail. It was shown in Section 3 that for $T \cong 1$ to 2×10^3 K an analytic approximation to $n_{He}(r_o, 180°)$ could be obtained. But since the temperature of the interstellar medium may well be as high as 5000 K, we have calculated $n_{He}(r_o, \Phi_o)$ for T = 5000 K by folding a Maxwellian velocity distribution function into the zero-temperature expression for n_{He} (r_o, Φ_o). Fahr [1971] has made a similar calculation for neutral hydrogen in the interplanetary medium.

Curves of angle-integrated flux F_v for counterclockwise and clockwise neutral He orbits and for T = 5000 K, $\langle V_\infty \rangle$ = 10 km/sec and $n_{He}(\infty)$ = 0.005 cm^{-3} are plotted in Figures 7 and 8, respectively. The sharp energy peaks are gone and the intensity scale is decreased by a factor of 10 with respect to Figures 4 and 5. If one ignores the low velocity parts of Figures 7 and 8 (which are most likely modified due to pitch-angle scattering in the interplanetary medium), the curves appear almost structureless, the only salient feature being a sharp high-velocity cut-off. To see if any annual structure remains with which to identify these fluxes as having an interstellar origin and also to try to determine the temperature T, we show in Figure 9 the summed fluxes for both clockwise and counterclockwise orbits as a function of Φ at the high-velocity cutoff point. It is seen that considerable annual variation remains with a peak-to-valley flux ratio of about 6:1 and a 2-month ($\Delta\Phi$ = 70°) full width at half maximum.

5. Discussion

In order to compare the expected fluxes of He^+ particles for different T, we show F_V as a function of V in Figure 10 for T = 100 K, 500 K and 5000 K, respectively, for a fixed observing position $\Phi = 190°$. Here only counterclockwise orbits are represented. A similar plot for $F_\phi(\phi)$ is shown in Figure 11. Both sets of curves are qualitatively similar and exhibit a rather large variation in the fluxes with temperature. As the temperature increases, both velocity and angle peaks disappear and the intensity diminishes. Thus, if the He^+ flux remains above instrument threshold sensitivities it might be possible to determine the temperature as well as the neutral He number density of the local interstellar medium.

To answer the first question posed in the introduction, we calculate the counting rates to be expected with an instrument similar in design to the Vela 5 and 6 heavy ion detectors. For T = 100 K, $\langle V_\infty \rangle$ = 10 km/sec and $n_{He}(\infty) = 0.005$ cm^{-3}, we obtain a peak counting rate of about 25 counts per peak energy sample. Similarly, for T = 500 K and 5000 K, we get 19.5 and 3.5 counts, respectively. Since the background count rate of the Vela 5 and 6 instruments is about 1/5 count per 112 msec sample time, statistically meaningful measurements can be made for 5000 K $\geq T \geq$ 100 K provided the He^+ fluxes can be separated from proton fluxes of solar wind origin and provided enough spectra are summed. The Vela 5 and 6 instruments were designed to detect heavy ions of solar origin and hence were not optimized for the detection of the He^+ particles considered here. One can gain from 1 to 2 orders of magnitude in count rate using existing instrumentation techniques.

We have presumed here a steady solar wind with V_{sw} = 400 km/sec, the magnetic field $\vec{B}$ aligned at the nominal spiral angle in the ecliptic plane and $\langle V_\infty \rangle$ = 10 km/sec, aligned in the ecliptic. Feldman et al. [1971]

studied the effect of variations of $\langle\vec{V}_\infty\rangle$ on the volume of occupation of He^+ particles in velocity space. They found only minor changes compared to the volume occupied. This means that it will be difficult to determine $\langle\vec{V}_\infty\rangle$ from measurements of the He^+ flux. But a large modification of the He^+ flux plotted in Figures 4 through 6 can result if $\langle\vec{V}_\infty\rangle$ is not oriented in the ecliptic, which is quite possible since the direction of $\langle\vec{V}_\infty\rangle$ is known only to within $\pm10°$ from Lyman-α measurements [Thomas, 1971]. This modification results from the fact that the high-density tail of the neutral He population is rather narrow for low temperatures (FWHM ≃ 6° for T = 100 K and $\langle V_\infty\rangle$ = 10 km/sec). Thus an observer of He^+ particles in the ecliptic may very well miss the tail region which is responsible for the sharp peaks plotted in Figures 4 through 6. This effect complicates the determination of $n_{He}(\infty)$ and T from He^+ observations in the ecliptic. A further complication arises from the strong dependence of the He^+ velocity space volume occupied on the direction of the interplanetary magnetic field $\vec{B}$. Observations of $\vec{B}$ at r = 1 AU show that although its average orientation is at the nominal spiral angle in the ecliptic, it is rarely found there. Even though the large amplitude, low frequency variations observed in the orientation of $\vec{B}$ do not scatter the He^+ particles considered here, they deform and tilt the phase space volume of occupation. In particular, orientation of $\vec{B}$ out of the ecliptic tilts the phase space volume accordingly, causing a misalignment of the acceptance fan of a hemispherical analyzer and the velocity circles occupied by the He^+ particles. One might then expect these particles to appear and disappear from view depending on whether $\vec{B}$ is oriented in or out of the ecliptic. Such an effect has been observed for bow-shock-accelerated protons observed upstream by Asbridge, Bame, and Strong [1968] and by Frank [1968].

6. Summary and Conclusions

To summarize, He^+ particles of interstellar origin in the solar wind are observable at 1 AU with present observation techniques. If the local interstellar medium is cold and $<\vec{V}_\infty>$ is aligned in the ecliptic, the observed He^+ fluxes should exhibit sharp peaks which vary systematically with the azimuthal observation position Φ about the sun. If the local interstellar medium is warm, He^+ fluxes should appear almost structureless except for a well-defined high-energy cutoff. The annual variation of He^+ flux at this cutoff should exhibit a peak in the anti-apex direction with peak-to-valley ratio of 6:1 and $\Delta\Phi_{FWHM} = 70°$ for T = 5000 K. Furthermore, fluxes of these particles are expected to be sporadic as orientations of $\vec{B}$ out of the ecliptic cause misalignment of the acceptance fan of a curved plate electrostatic analyzer with the He^+ velocity circles. Lastly, measurements in a near-earth orbit are complicated by bow-shock-accelerated particles which have been observed by Asbridge, et al. [1968] and Frank [1968] to have similar characteristics and, within an order of magnitude, the same flux as expected from the He^+ particles of interstellar origin. In spite of these difficulties, a separation of bow-shock proton and interstellar He^+ fluxes may be experimentally possible due to differences in velocity space volumes occupied as well as differences in annual variations.

Acknowledgments

We wish to thank M. Montgomery for useful discussions. This work was supported in part by the National Aeronautics and Space Administration under research grant NGR 50-002-162 and contract NAS2-6759.

References

Asbridge, J. R., S. J. Bame, and I. B. Strong, Outward flow of protons from the earth bow shock, J. Geophys. Res., 73, 5777, 1968.

Axford, W. I., The interaction of the solar wind with the interstellar medium, Proc. of the Solar Wind Conference, Asilomar, Pacific Grove, California, 1971.

Bertaux, J. L. and J. E. Blamont, Evidence for a source of an extraterrestrial hydrogen Lyman-alpha emission: the interstellar wind, Astron. and Astrophys., 11, 200, 1971

Danby, J. M. A., and G. L. Camm, Statistical dynamics and accretion, Monthly Notices Roy. Astron. Soc., 117, 50, 1957.

Danby, J. M. A. and T. A. Bray, Density of interstellar matter near a star, Astron J., 72, 219, 1967.

Fahr, H. J., The interplanetary hydrogen cone and its solar cycle variations, Astron. and Astrophys., 14, 263, 1971.

Feldman, W. C., J. J. Lange, and F. Scherb, Interstellar helium in interplanetary space, Proc. of the Solar Wind Conf., Asilomar, Pacific Grove, California, 1971.

Frank, L. A., Observation of low-energy protons and electrons with IMP 4 (abstract), Trans. Am. Geophys. Union, 49, 738, 1968.

Holzer, T. E. and W. I. Axford, Interaction between interstellar helium and the solar wind, J. Geophys. Res., 76, 6965, 1971.

Thomas, G. E., Properties of nearby interstellar hydrogen deduced from Lyman-alpha sky background measurements, Proc. of the Solar Wind Conference, Asilomar, Pacific Grove, California, 1971.

Thomas, G. E. and R. F. Krassa, OGO 5 measurements of the Lyman-alpha sky background, Astron. and Astrophys., 11, 218, 1971.

Figure Captions

Fig. 1 The interstellar infall coordinate system with $\langle\vec{V}_\infty\rangle$ in the ecliptic.

Fig. 2 The projection onto the ecliptic of the He^+ velocity distribution function. The lines, in order from longest to shortest in each sequence drawn perpendicular to $\vec{B}$ represents the diameter of a circle about $\vec{B}$ corresponding to He^+ ions injected into the solar wind at r_o = 1.0, 0.9, 0.8, 0.7, 0.6, 0.5, 0.4, and 0.3 AU, respectively. The circle about a radial velocity of 400 km/sec represents the projection of a sphere with radius, V_{th} = 40 km/se .

Fig. 3 A view of the He^+ velocity distribution function in a plane perpendicular to $\vec{B}$. The spherical velocity wedge represents a typical volume accepted by the Vela 5 or 6 heavy ion detectors.

Fig. 4 The angle integrated fluxes of He^+ particles from the outer 36° of those velocity circles of the sequence of circles resulting from counterclockwise neutral He orbits. Here $n_{He}(\infty) = 0.005\ cm^{-3}$, $\langle V_\infty\rangle$ = 10 km/sec and T = 100°K. The separate curves are for various ecliptic observation longitudes, Φ.

Fig. 5 The angle integrated fluxes of He^+ particles from the outer 36° of those velocity circles of the sequence of circles resulting from clockwise neutral He orbits. Here $n_{He}(\infty) = 0.005\ cm^{-3}$, $\langle V_\infty\rangle$ = 10 km/sec and T = 100°K. The separate curves are for various ecliptic observation longitudes.

Fig. 6 The velocity integrated fluxes of He^+ particles from the outer 36° of those velocity circles of the sequence of circles resulting from counterclockwise neutral He orbits. Here $n_{He}(\infty) = 0.005\ cm^{-3}$, $\langle V_\infty\rangle$ = 10 km/sec, and T = 100°K. The separate curves are for various ecliptic observation longitudes, Φ.

Fig. 7 A plot identical to Figure 4 but for T = 5000°K.

Fig. 8 A plot identical to Figure 5 but for T = 5000°K.

Fig. 9 The annual variation of the He^+ particle flux summed for both clockwise and counterclockwise neutral He orbits at the high velocity cutoff points in Figures 7 and 8.

Fig. 10 The variation of the angle integrated He^+ flux distribution with T for a fixed observing position $\Phi = 190°$.

Fig. 11 The variation of the velocity integrated flux distribution with T for a fixed observing position $\Phi = 190°$.

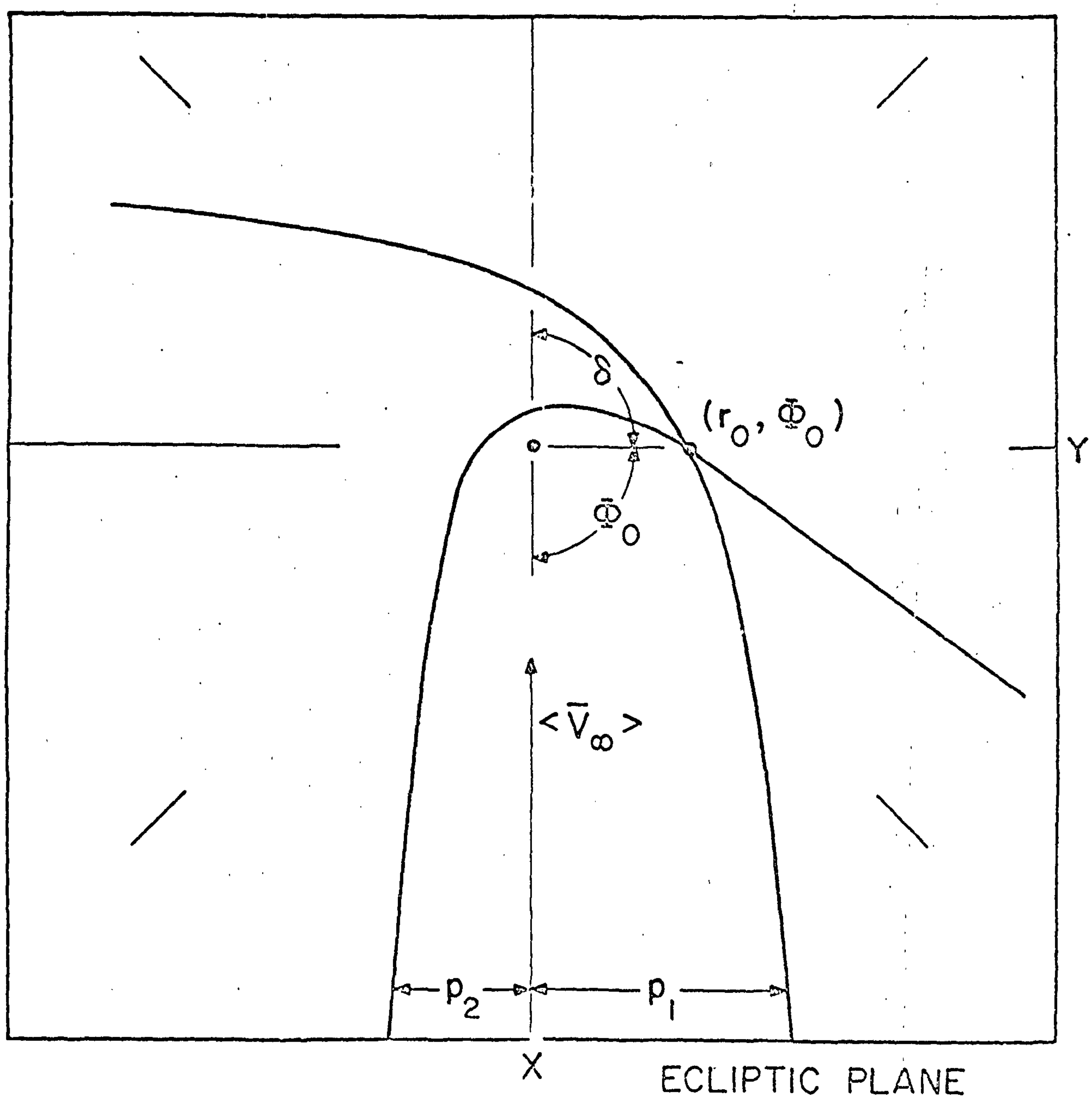

Fig. 1

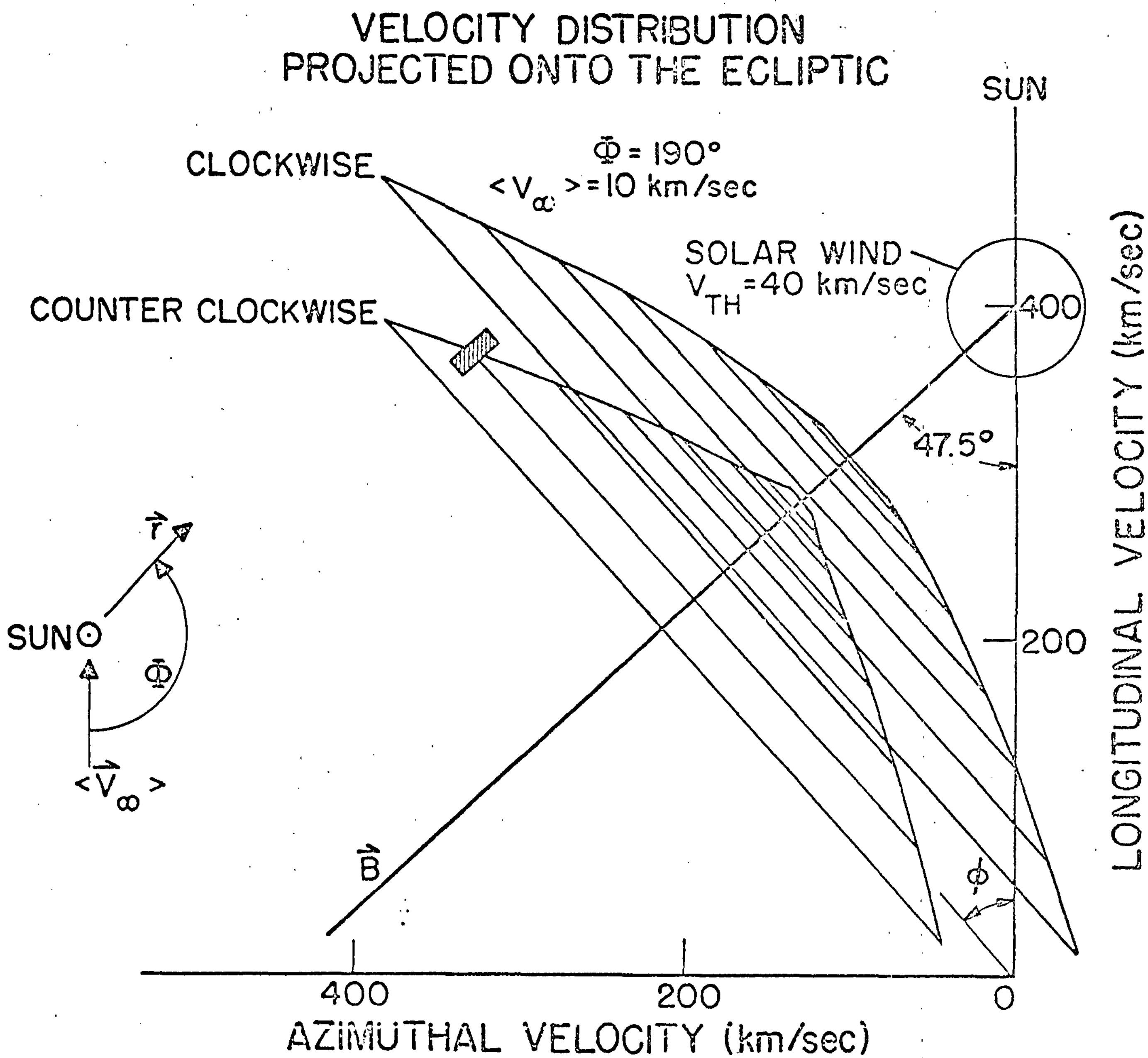

VELOCITY DISTRIBUTION
PROJECTED ONTO THE ECLIPTIC
SUN
CLOCKWISE
$\Phi = 190°$
$< V_{\alpha} > = 10$ km/sec
SOLAR WIND
$V_{TH} = 40$ km/sec
COUNTER CLOCKWISE
400
47.5°
SUN
$\vec{r}$
Φ
$< \vec{V}_{\infty} >$
200
$\vec{B}$
ϕ
400
200
0
AZIMUTHAL VELOCITY (km/sec)
LONGITUDINAL VELOCITY (km/sec)

Fig. 2

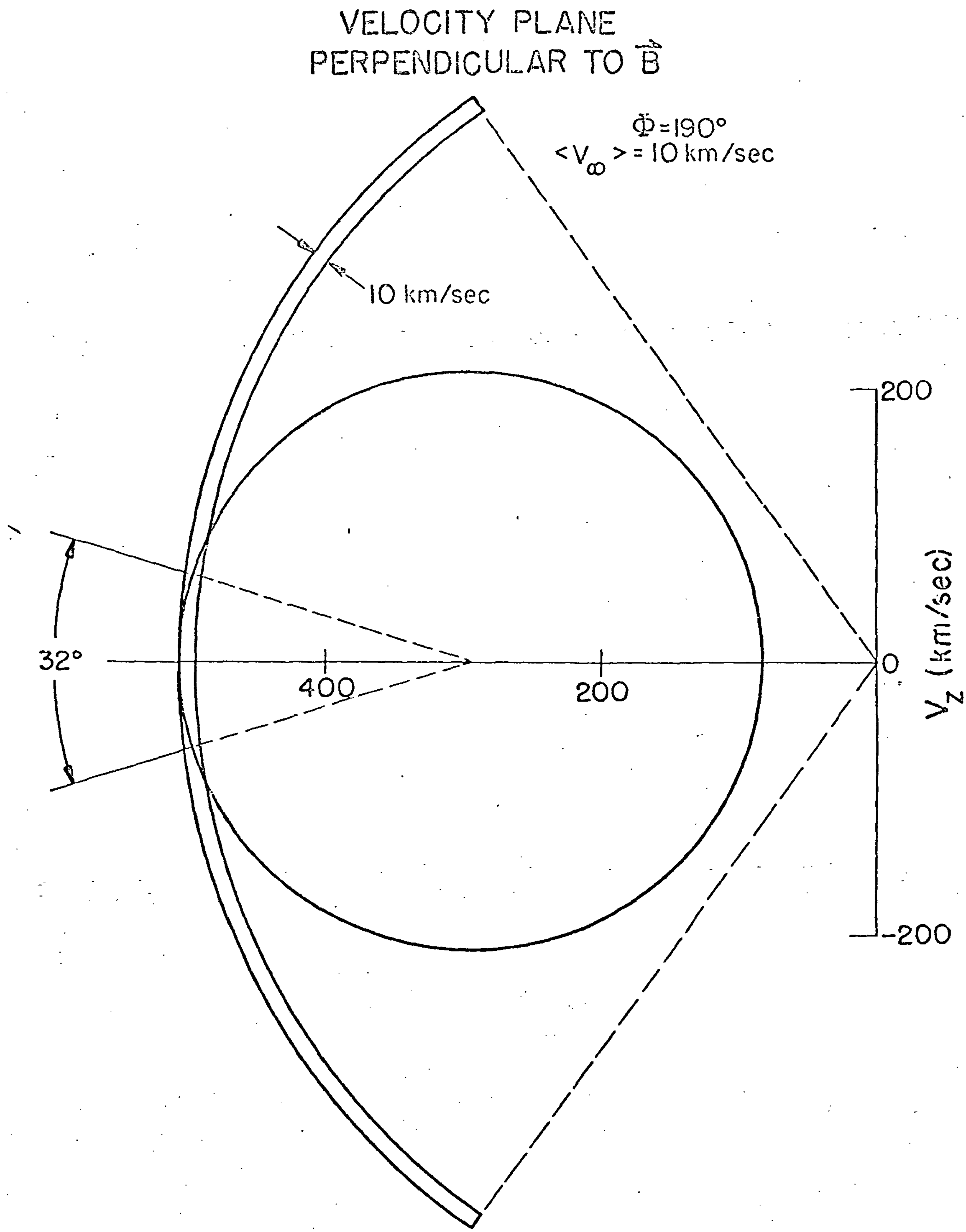

VELOCITY PLANE
PERPENDICULAR TO $\vec{B}$
Φ=190°
<V_∞> = 10 km/sec
10 km/sec
32°
400
200
200
0
-200
V_z (km/sec)

Fig. 3

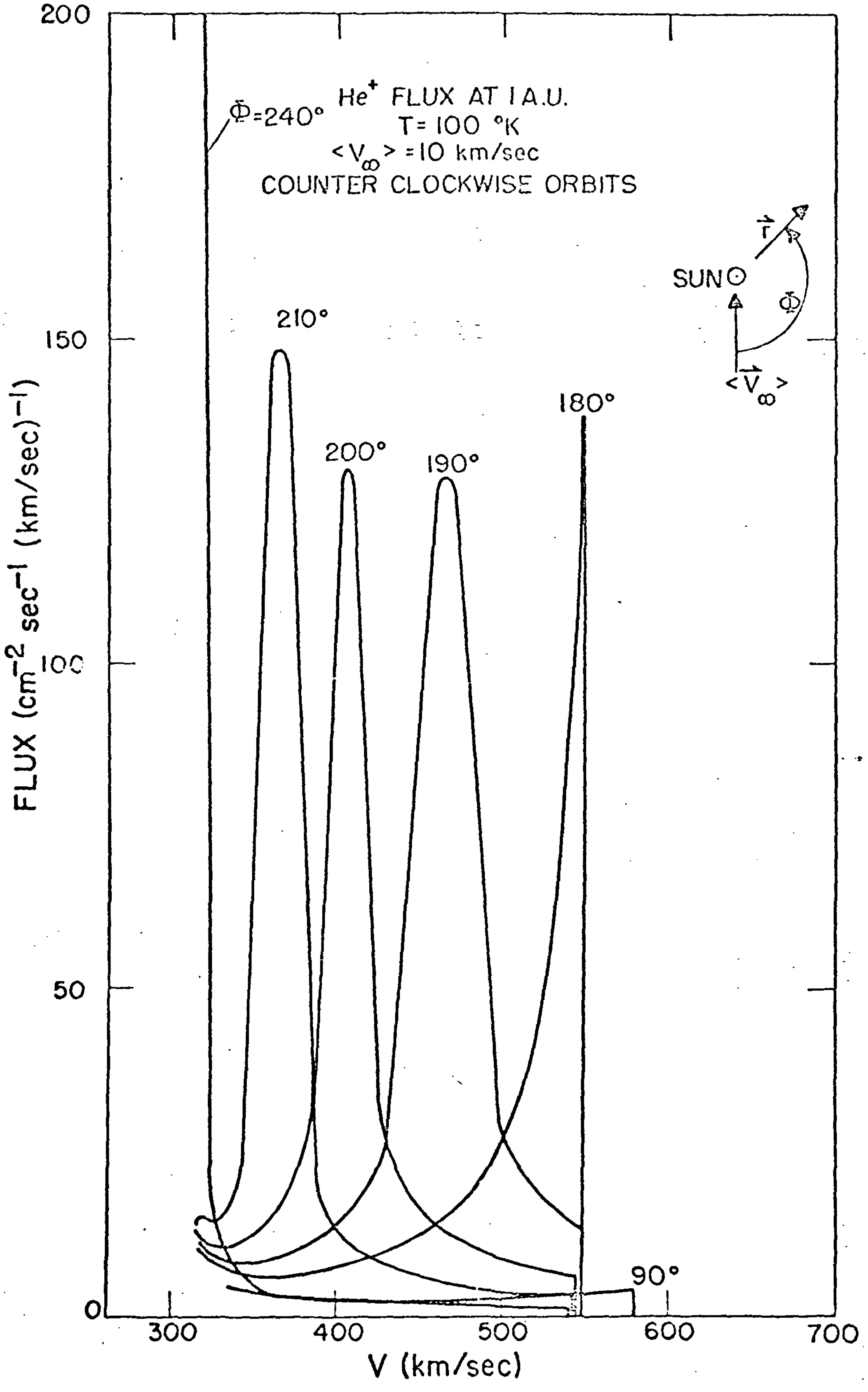
He+ FLUX AT 1 A.U.
T= 100 °K
<V∞> = 10 km/sec
COUNTER CLOCKWISE ORBITS
Φ=240°
210°
200°
190°
180°
90°
SUN
r
Φ
<V∞>
FLUX (cm-2 sec-1 (km/sec)-1)
V (km/sec)
200
150
100
50
0
300
400
500
600
700

Fig. 4

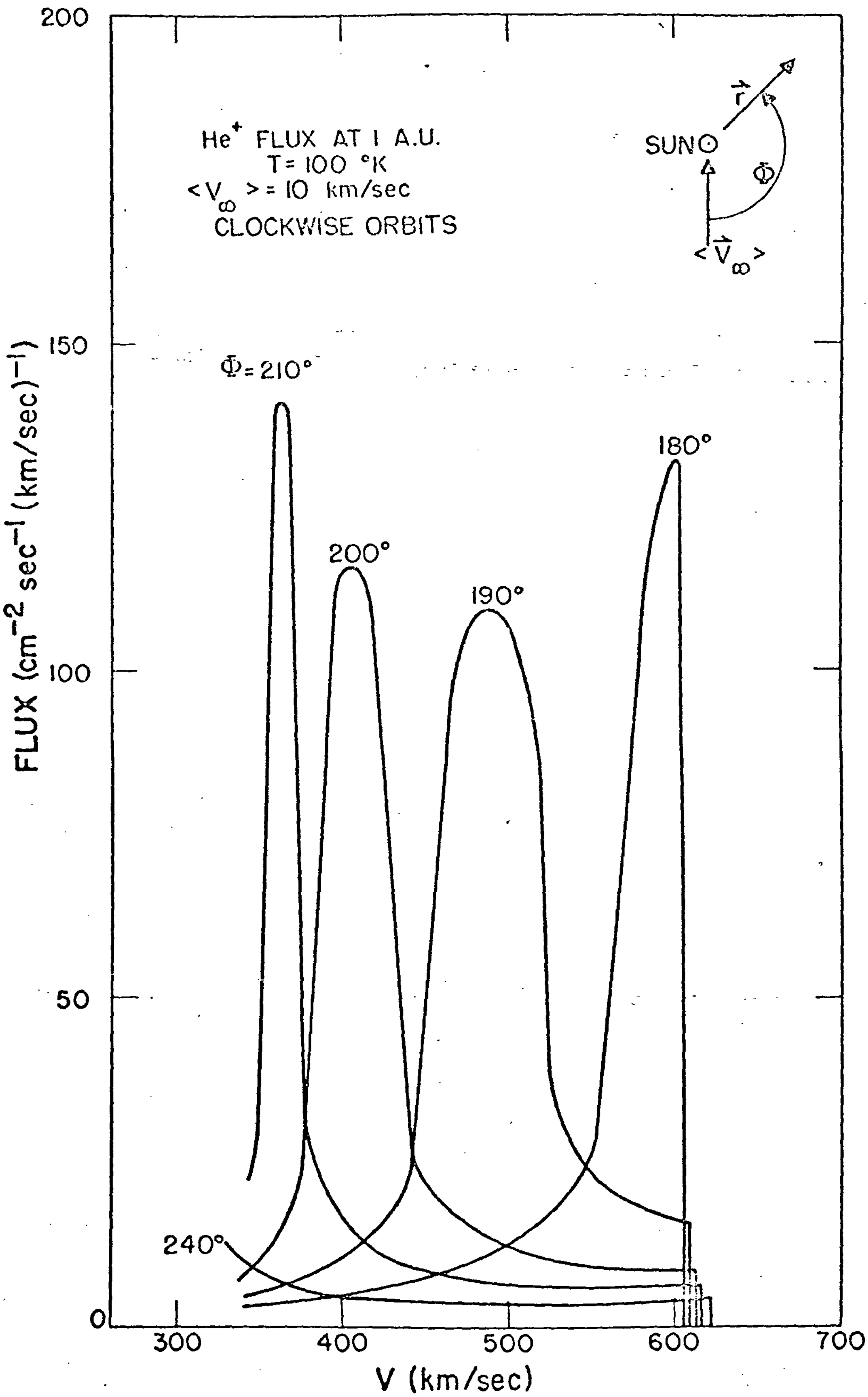
He+ FLUX AT 1 A.U.
T = 100 °K
<V∞> = 10 km/sec
CLOCKWISE ORBITS
SUN
r
Φ
<V∞>
Φ = 210°
200°
190°
180°
240°
FLUX (cm-2 sec-1 (km/sec)-1)
V (km/sec)
200
150
100
50
0
300
400
500
600
700

Fig. 5

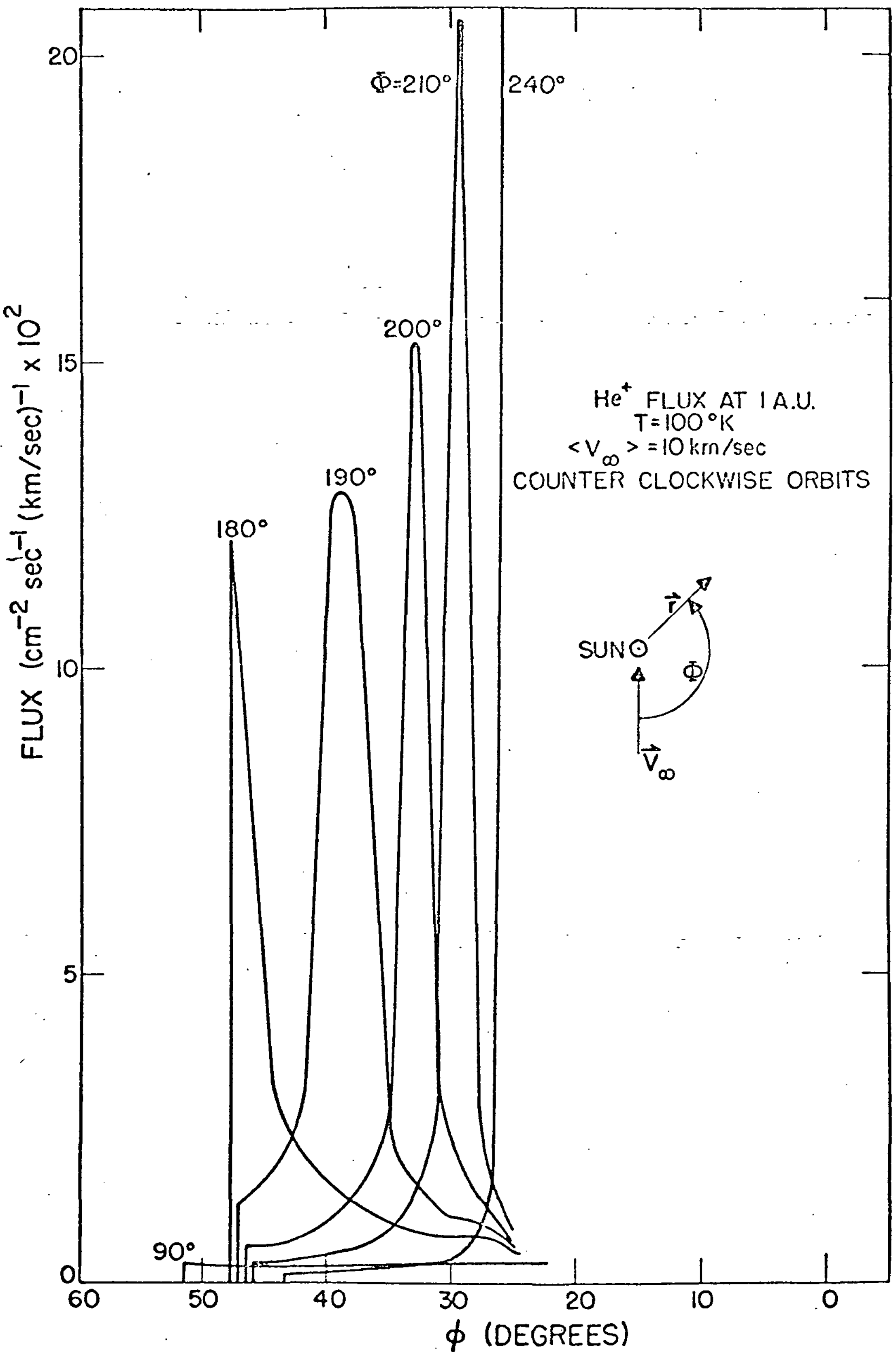

20
15
10
5
0
60
50
40
30
20
10
0
FLUX (cm^{-2} sec^{-1} (km/sec)$^{-1}$ x 10^{2}
φ (DEGREES)
Φ=210°
240°
200°
190°
180°
90°
He^{+} FLUX AT 1 A.U.
T=100°K
<V$_\infty$> =10 km/sec
COUNTER CLOCKWISE ORBITS
SUN
r
Φ
V$_\infty$

Fig. 6

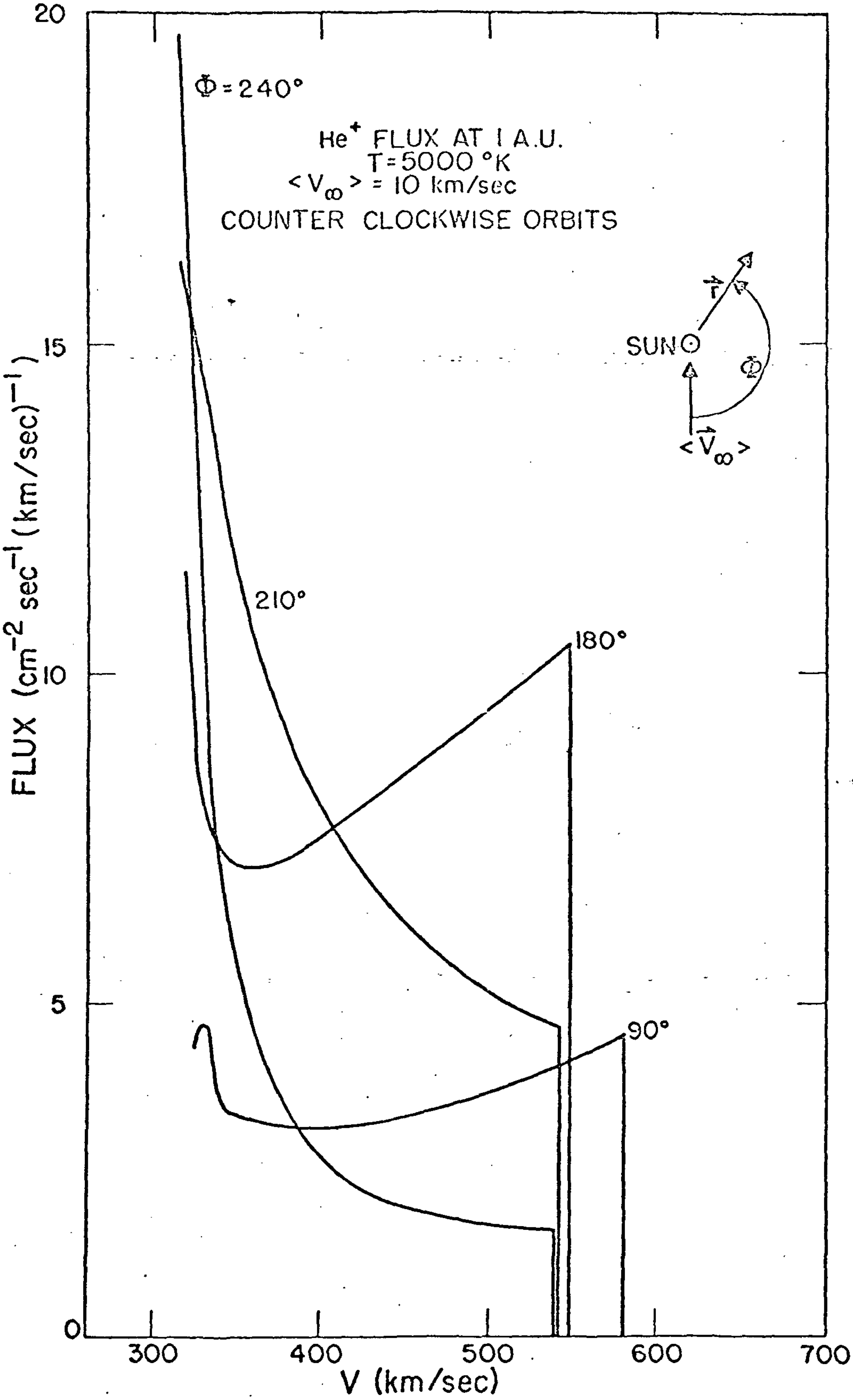

Φ=240°
He+ FLUX AT 1 A.U.
T=5000 °K
<V∞> = 10 km/sec
COUNTER CLOCKWISE ORBITS
SUN
r
Φ
<V∞>
210°
180°
90°
FLUX (cm⁻² sec⁻¹ (km/sec)⁻¹)
V (km/sec)
20
15
10
5
0
300
400
500
600
700

Fig. 7

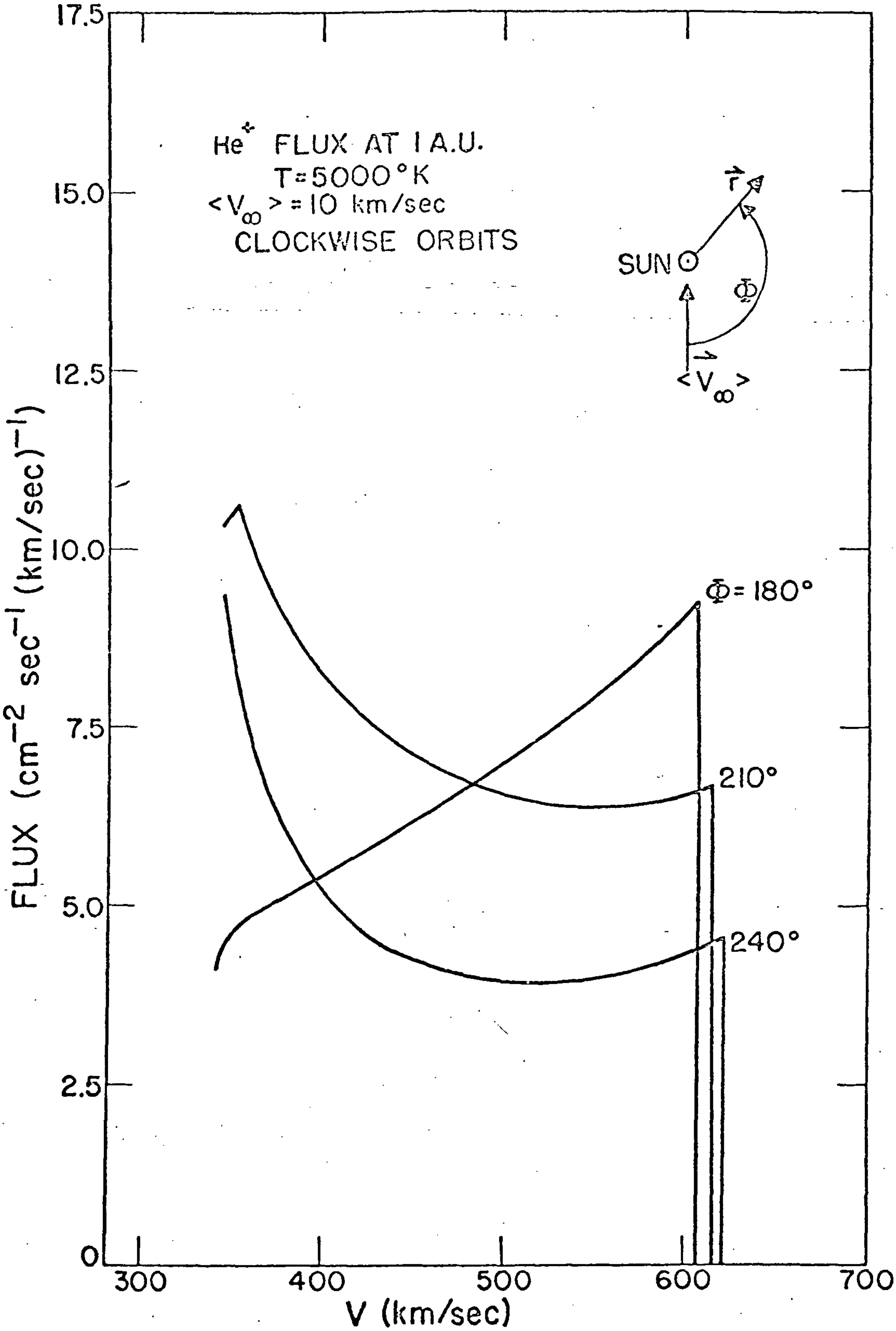
He+ FLUX AT 1 A.U.
T=5000°K
<V∞> = 10 km/sec
CLOCKWISE ORBITS
SUN
r
Φ
<V∞>
Φ = 180°
210°
240°
FLUX (cm⁻² sec⁻¹ (km/sec)⁻¹)
V (km/sec)
17.5
15.0
12.5
10.0
7.5
5.0
2.5
0
300
400
500
600
700

Fig. 8

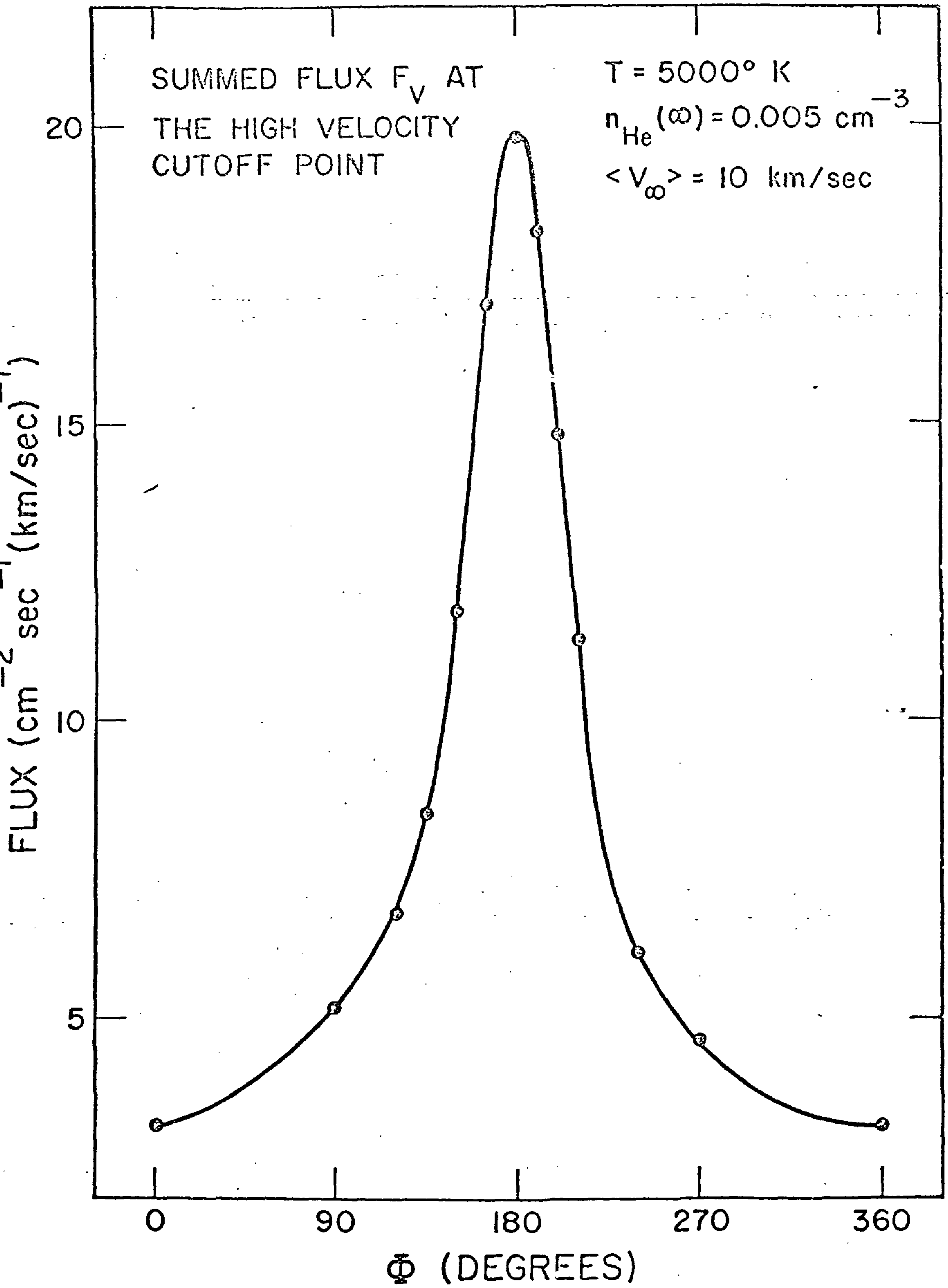
SUMMED FLUX F_V AT
THE HIGH VELOCITY
CUTOFF POINT
T = 5000° K
n_He(∞) = 0.005 cm^-3
<V_∞> = 10 km/sec
FLUX (cm^-2 sec^-1 (km/sec)^-1)
20
15
10
5
0
90
180
270
360
Φ (DEGREES)

Fig. 9

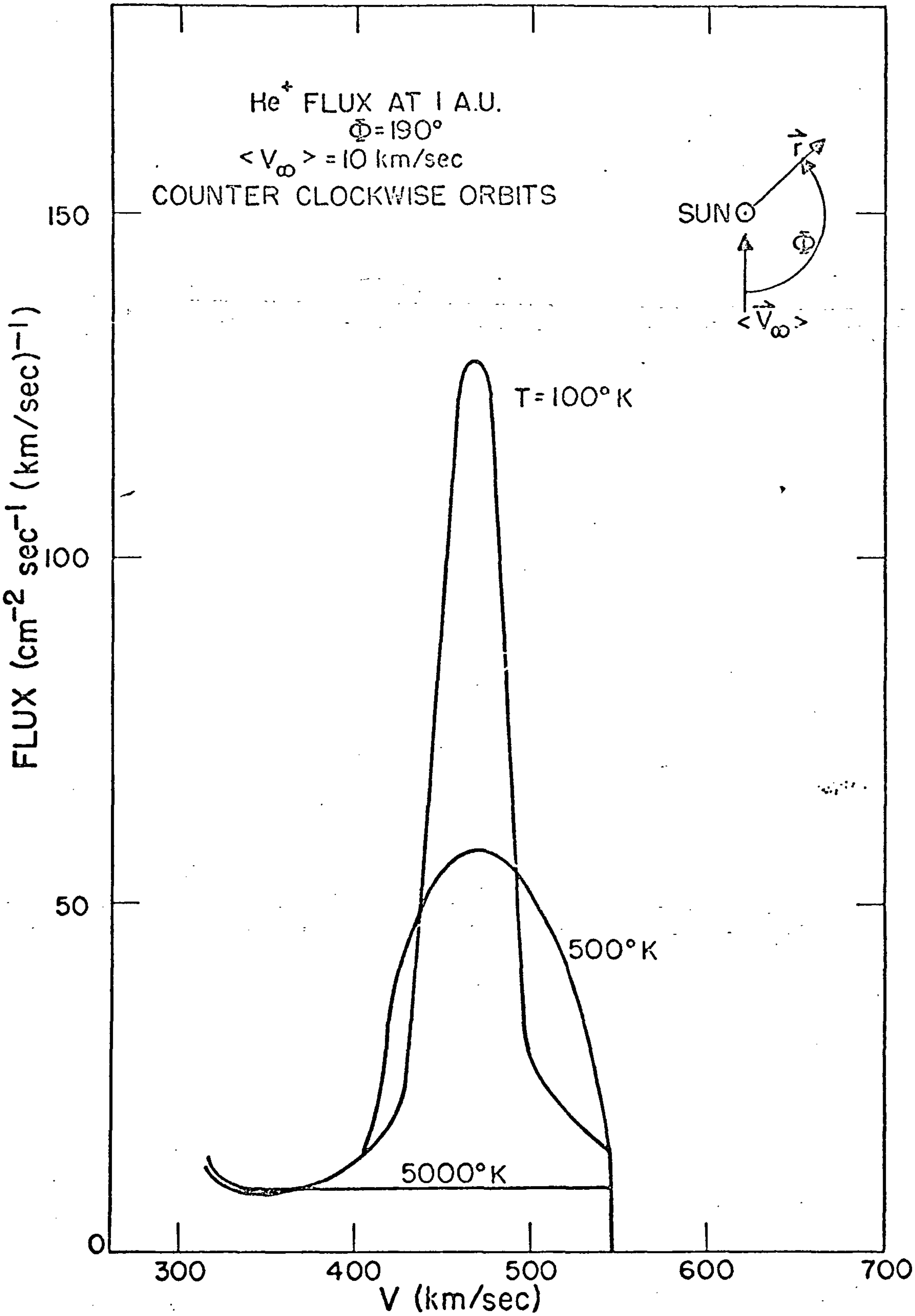
He+ FLUX AT 1 A.U.
Φ=190°
<V∞> = 10 km/sec
COUNTER CLOCKWISE ORBITS
SUN
r
Φ
<V∞>
T=100°K
500°K
5000°K
FLUX (cm-2 sec-1 (km/sec)-1)
150
100
50
0
300
400
500
600
700
V (km/sec)

Fig. 10

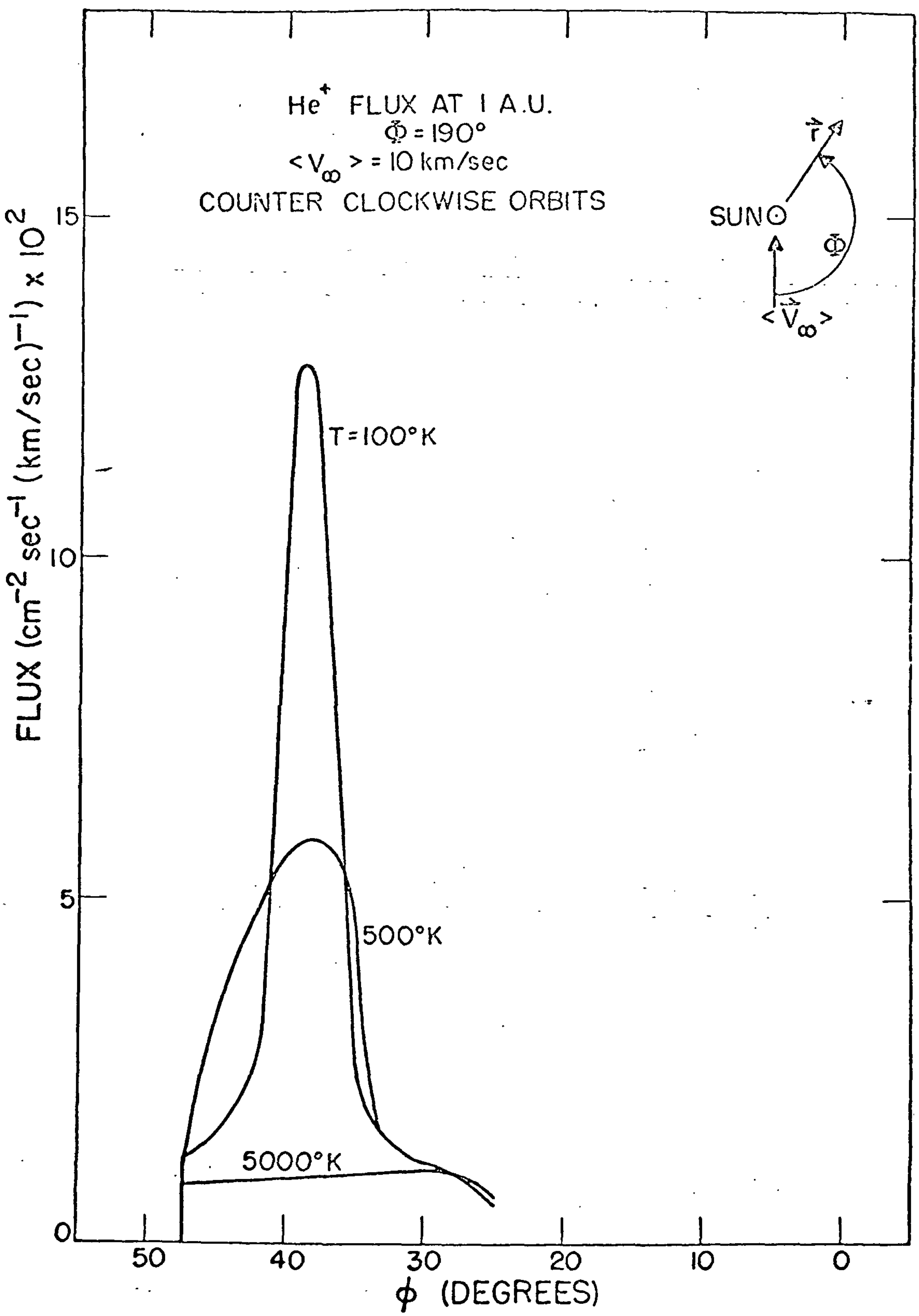
He+ FLUX AT 1 A.U.
Φ = 190°
<V∞> = 10 km/sec
COUNTER CLOCKWISE ORBITS
SUN
r
Φ
<V∞>
T=100°K
500°K
5000°K
FLUX (cm-2 sec-1 (km/sec)-1) x 10^2
15
10
5
0
50
40
30
20
10
0
φ (DEGREES)

Fig. 11

APPENDIX C

LOW INTENSITY BALMER EMISSIONS FROM THE INTERSTELLAR MEDIUM AND GEOCORONA

R. J. Reynolds*
NASA, Goddard Space Flight Center
Greenbelt, Maryland

and

F. L. Roesler and F. Scherb
Physics Department, University of Wisconsin
Madison, Wisconsin

Received: ________________

*National Academy of Sciences Resident Research Associate

LOW INTENSITY BALMER EMISSIONS FROM THE INTERSTELLAR MEDIUM AND GEOCORONA

ABSTRACT

Galactic and non-galactic components of the diffuse Hα and Hβ night sky emissions have been resolved with a Fabry-Perot spectrometer. The non-galactic component of both lines accounts for most of the emission at galactic latitudes greater than 30^{o}. The intensities of the galactic component yield values for the average ionization rate per hydrogen atom that are between 10^{-15} and $10^{-14} s^{-1}$ assuming steady-state ionization.

I. INTRODUCTION

A study of faint, diffuse galactic Hα and Hβ emissions has been started using a 150 mm diameter Fabry-Perot spectrometer at the coude focus of the 36-inch telescope at Goddard Space Flight Center in Maryland. The spectrometer has a spectral resolving power of 25,000 (12 km/s) and a circular 6.5' field of view. Faint Hβ emissions that do not appear to be associated with any known HII regions have previously been observed by Johnson (1971) using interference filters and by Daehler et al. (1968) and Reay and Ring (1969) using Fabry-Perot spectrometers, but low spectral resolution prevented them from being able to discriminate between galactic and possible local emission sources. Since the galactic hydrogen often has radial velocities of ± 25 km/s or more with respect to the earth, it has been possible with the present spectrometer's 12 km/s resolution to resolve the unshifted (probably geocoronal) Hα and Hβ lines from the galactic lines, and thus unambiguously determine for a variety of observation directions the relative contributions of each source to the line intensites.

II. OBSERVATIONS

Figure 1 shows two Hβ scans in a direction of low galactic latitude ($l^{II} = 184.5^o$, $b^{II} = -5.8^o$) at two different times of the year. The photomultiplier count rates are plotted as a function of the radial velocity with respect to the earth. In Figure 1a the galactic local standard of rest (LSR) velocity was at -11 km/s and there appeared to be a single Hβ line. Three months later (Figure 1b) the LSR velocity has shifted to +30 km/s with respect to the earth and there appeared two clearly resolved lines -- a galactic Hβ line near the LSR velocity and a fainter, narrower Hβ line at 0 km/s. Scans of the Hα lines in this direction are shown in Figure 2. Unfortunately the galactic Hα line at +35 km/s in these two scans is nearly obscured by an OH airglow line leaking through a side transmission peak of the Fabry-Perot etalon.

Using the absolute Hα and Hβ intensity measurements of HII regions (Ishida and Kawajii 1968; Boyce 1966; O'Dell, et al. 1967; Schmitter 1971) and planetary nebulae (Collins, et al. 1960), the non-galactic and galactic Hβ emission lines in Figure 1b were found to have intensities of 0.3-0.4 R and 0.6-0.8 R respectively (1R = 8 x 10^4 photons/cm^2sec sterad). The unshifted Hα lines in Figures 2a and 2b have intensities of 1.5-2.0 R and 3.2-4.5 R respectively. The line widths imply temperatures lower than 1500^oK

for the non-galactic source and 5500 ± 1500°K for the galactic source assuming that the widths are due to thermal motions only.

a) Non-Galactic Balmer Emissions

Observations have been made in more than 40 directions between 1971 October and 1972 March. The non-galactic Hα and Hβ lines are centered (to within a 2 km/s measurement accuracy) on 0 km/s, and both have line widths implying a temperature lower than 1500°K for the emitting region.

Figure 3 demonstrates how the observed intensities of these lines varied with changing geometry between the observation direction and the sun. The count rates above background at the peak of the line are plotted as a function of the angle θ between the observation direction and the direction to the sun. The Hα and Hβ count rates obtained on various dates between January and March 1972 in a single low galactic latitude direction ($l^{II} = 184.5^{o}$, $b^{II} = -5.8^{o}$) are plotted together with the Hβ rates observed in a variety of directions (and solar depression angles) during a single night on 1971 November 21-22. The rates have been normalized for equal atmospheric transmission. The data in Figure 3 indicate that: (1) the Hβ intensity has remained virtually constant between 1971 November and 1972 March for $\theta \geq 90^{o}$; (2) although the Hα intensity does vary significantly with changing geometry as has been observed before by others and is easily explained by the scattering of solar Lβ in the geocorona, the Hβ intensity for $\theta \geq 90^{o}$ appears to be quite independent of θ, as well as solar depression angle as is seen from the lack of significant scatter of the points about the dashed line. This result is difficult to explain by scattering of solar Lγ in the geocorona, since in such a case the

$H\beta$ intensity should continue to decrease with increasing θ beyond 90^{o} because fewer $L\gamma$ photons can be scattered into these directions. Reay and Ring (1969) observed similar behavior for $H\beta$ emission at high galactic latitudes using a Fabry-Perot spectrometer with relatively low (36 km/s) resolution. However, even though they were not able to spectrally eliminate possible galactic contributions, their quoted absolute intensities are a factor of 3 or 4 times lower than those presented here. This discrepancy may be evidence of significant changes in the intensity of the $H\beta$ line over a period of years.

Both the narrow line width and the 0 km/s radial velocity eliminate the possibility that this emission is due to either interplanetary hydrogen or tropospheric scattering of bright astronomical sources (Tinsley 1970). Also neither line was present in the spectrum of scattered terrestrial lights. Therefore, the origin of both lines, $H\beta$ as well as $H\alpha$, is probably the geocorona. The uniform, bright 0.5 R $H\beta$ flux for $\theta \geq 90^{o}$ as well as the low absolute $H\alpha$:$H\beta$ ratio of 4-5:1 for the $\theta = 143^{o}$ observation suggest then that perhaps there is a second Balmer line producing mechanism in the geocorona (Kondo and Kupperian 1967) in addition to the excitation of hydrogen by direct and scattered solar Lyman radiation. More careful measurements of the positions of these lines may help determine the mechanism of excitation. Balmer lines which are produced by absorption of Lyman radiation involve only the transitions $n^2P - 2^2S$. Such lines will have an apparent blue shift of approximately 2 km/s with respect to lines produced as a result of recombination radiation.

b) Galactic Balmer Emissions

From observations in more than 40 directions covering galactic latitudes -60° to $+87^{\circ}$ and galactic longitudes 60° to 250°, it appears that, with a few possible exceptions, the unshifted (geocoronal) lines account for nearly all the $H\alpha$ and $H\beta$ emissions from directions more than 30° from the galactic plane. An $H\beta$ scan at $+23^{\circ}$ galactic latitude and an $H\alpha$ scan near the galactic pole, shown in Figures 4a and 4b respectively, are typical of data from high galactic latitudes. The excess emission on the blue side of the unshifted $H\beta$ line in Figure 4a indicates the presence of galactic $H\beta$ emission (0.3-0.7 R) from this direction. No such asymmetry is apparent in the $H\alpha$ line in Figure 4b, implying a galactic $H\alpha$ intensity $I\alpha < 0.4R$ in the galactic pole direction. Since the LSR velocity is rarely shifted by more than about ± 40 km/s from the laboratory velocity, the study of the galactic Balmer emissions at high galactic latitudes will often be limited to observations of asymmetries in the wings of the unshifted geocoronal lines.

III. THE INTERSTELLAR MEDIUM

Observations of diffuse galactic Balmer lines can be used to determine various properties of the interstellar medium. In directions of low visual extinction, or where the extinction is well known, the intensity $I\beta$ of the galactic $H\beta$ emission can be used (assuming steady-state) to determine the average ionization rate per hydrogen atom $\langle\zeta_H\rangle$ along the line of sight, given by the relation (Reynolds et al. 1971, hereafter referred to as Paper I)

$$\langle\zeta_H\rangle = 105\ I\beta/N_H \qquad (1)$$

where N_H is the columnar atomic hydrogen density in units of cm^{-2} and $I\beta$ is in units of photons $cm^{-2} s^{-1} sterad^{-1}$. The emission measure e.m., can also be computed (Paper I) from $I\beta$ and an estimate of the temperature, which can be obtained from the line width, when observable, and assumed contributions of turbulence. (Upper limits to the temperature and emission measure can always be obtained from the line width by assuming thermal broadening only.) When the observations are made in directions near pulsars, the pulsar dispersion measure d.m. can be combined with e.m. (or only an upper limit on e.m.) to set both a lower limit on the total distance L along the line of sight occupied by the ionized hydrogen, given by (Paper I)

$$L \geq (\text{d.m.})^2/\text{e.m.}, \qquad (2)$$

and an upper limit on the average electron density $\langle n_e \rangle$ within the regions of ionization, given by (Paper I)

$$\langle n_e \rangle \leq \text{e.m./d.m.} \qquad (3)$$

Table 1 summarizes the results of applying this analysis to the three observation directions discussed above. For the low-galactic-latitude direction which is near the Crab Nebula pulsar, two separate cases were considered. In column (a) the emission was assumed to be originating from a single localized region well within one $H\beta$ mean free path length (1 kpc) of the sun so that turbulent velocities and extinction could be neglected. However, the resulting large lower limit on L suggests that the region may not be localized. Therefore, in column (b) the emission was assumed to be originating from a large number of regions distributed uniformly along the total line of sight distance through the galactic disk. The random velocity distribution of these regions was assumed to have a FWHM of 7 km/s -- a value derived from the random motions of the HI clouds since broadening due to galactic rotation is negligible in this near anti-center direction. It should be noted that even if non-thermal velocity contributions to the observed line width were greater than 7 km/s, resulting in a lower temperature and lower emission measure for the emitting region, the value of $<\zeta_H>$ would remain unchanged and the limits on $<n_e>$ and L would become even more stringent, i.e., the upper limit on $<n_e>$ would decrease and the lower limit on L would increase. Corrections for extinction were made using data given by O'Dell (1962) for this direction. Since there are two pulsars near this direction -- the Crab pulsar NP 0532 (9' West) with d.m. = 57 cm^{-3}pc and NP 0527 (1.5^o West) with d.m. = 51 cm^{-3}pc -- the smaller dispersion measure was chosen in the computations; the difference between the two values was assumed to be due to the Crab Nebula.

Columns (c) and (d) of Table 1 summarize the observational data in the two higher galactic latitude directions. Since no line profiles were obtained in these directions, in order to compute e.m. the temperature was assumed to be approximately the same (5000^{o}K) as in the low latitude direction. But as mentioned above, the limits on $<n_e>$ and L values of $<\zeta_H>$ continue to hold for any temperature less than 5000^{o}K. Note also that even though no galactic emission was detected from the galactic pole direction, the value of the pulsar dispersion measure and the upper limit on Iα still allow limits to be placed on e.m., $<n_e>$, L, and $<\zeta_H>$ in this direction.

The data in Table 1 indicate that in the two directions near pulsars where limits could be placed on L and $<n_e>$, the regions of ionization occupy a considerable fraction of the line of sight distance through the galactic disk with $<n_e> \leq 0.1$ cm^{-3}. A value of $<\zeta_H>$ of about 3 x 10^{-15}/sec H-atom is consistent with the data in all three directions. However, in other directions (to be discussed below) where the diffuse galactic emission is brighter, values for $<\zeta_H>$ are as high as 20-30 x 10^{-15}/sec H-atom.

With the limited number of observations, the large-scale structure of the galactic Balmer emission is not yet clear. The only region of the galactic plane that has been studied in any detail is the region near the galactic anticenter ($160^\circ < l^{II} < 200^\circ$ and $-20^\circ < b^{II} < +10^\circ$). Figure 5 is a map of this region in galactic coordinates denoting the observation directions (open circles) and the brightness contours (solid lines) around the brighter regions of the diffuse galactic H_β emission. In the directions outside the contour lines, faint galactic emission appears to be present with intensities of approximately 0.3R to 1.0R. The large "bright" region emphasized by the contour lines could be part of a very large region of ionization surrounding the Orion association (outlined by a dashed oval). Another large region of ionization appears to be present in the Cygnus region of the galactic plane between galactic longitudes 70° and 100°. This region has also been observed by Montbriand, et al. (1965) and Courtes and Sivan (1972) using photographic methods. It is important to determine whether these regions are isolated anomalies superimposed upon a fainter, more uniform emission whose intensity is strongly correlated with N_H (in directions of low extinction), or whether all the diffuse Balmer emission is the result of a superposition of many of these regions filling the galactic disk. The former case would suggest a steady-state ionization process involving cosmic rays, x-rays, or UV photons (Hawakawa *et al.* 1961; Silk and Werner 1970; Walmsley and Grewing 1971), while the latter case would suggest possible non-steady-state processes (Bottcher *et al.* 1970).

In an effort to resolve these questions, a more extensive survey is planned, and additional interstellar emission lines will be studied including the [OIII] 5007Å line and lines of HeI.

We are grateful to John Trauger for his work on the optical coatings and to Dr. E. Boldt for helpful discussions. This work has been supported in part by the National Academy of Sciences through a resident research associateship, by the National Aeronautics and Space Administration through grant NGL 50-002-162, by the Atmospheric Sciences Section, National Science Foundation through grant GA-15733, and by the University of Wisconsin Graduate School through funds provided by the Wisoonsin Alumni Research Foundation.

TABLE 1

PROPERTIES OF THE INTERSTELLAR MEDIUM
IN THREE SELECTED DIRECTIONS

	$b = -5.8^{\circ}$ $l = 184.5^{\circ}$		$b = +23^{\circ}$ $l = 178^{\circ}$	$b = +86.5^{\circ}$ $l = 253^{\circ}$
	NP 0532 and NP 0527		-	PSR 1237
Parameters	a	b	c	d
d.m. ($cm^{-3}pc$).........	51.	51.	-	8.5
N_H ($X10^{-20}cm^{-2}$).......	44.	44.	7.	2.3*
$T(^{o}K)$.................	5500 ± 1500	4000 ± 1500	5000†	5000†
Iβ (R) (galactic).....	0.7 ± 0.2	0.7 ± 0.2	0.4 ± 0.2	-
Iα (R) (galactic).....	-	-	-	<0.4
e.m. ($cm^{-6}pc$).........	4. ± 1.	8. ± 2.	2. ± 1.	<0.6
$<n_e>$ (cm^{-3})...........	≤0.08 ± 0.02	≤0.2 ± 0.1	-	<0.1
L (pc)................	≥600 ± 200	≥300 ± 100	-	>100
$<\zeta_H>$($X10^{15}$/H-atom sec)	-	3. ± 1.	4. ± 2.	<4.

* interpolated from measurements 4° away

† assumed (not measured)

REFERENCES

Bottcher, C., McCray, R. A., Jura, M., and Dalgarno, A. 1970, Astrophys. Let., 6, 237.

Boyce, B. 1966, Lowell Observatory Bull. No. 130, 215.

Collins II, G. W., Daub, C. T., and O'Dell, C. R. 1960, Ap. J., 133, 471.

Courtes, G. and Sivan, J. P. 1972, preprint.

Daehler, M., Mack, J. E., Stoner, Jr., J. O., Clark, D., and Ring, J. 1968, Planet. Space Sci., 16, 795.

Hayakawa, S., Nishimura, S., and Takeyanagi, K. 1961, Publ. Astr. Soc. Japan, 13, 184.

Ishida, K., and Kawajiri, N. 1968, Publ. Astr. Soc. Japan, 20, 95.

Johnson, H. M. 1971, Ap. J. 164, 379.

Kondo, Y. and Kupperian, Jr., J. E. 1967, J. Geophys. Res., 72, 6091.

Montbriand, L. E. J., Tinsley, B. A., and Jones, A. 1965, Can. J. Phys., 43, 782.

O'Dell, C. R. 1962, Ap. J., 136, 809.

O'Dell, C. R., York, G., and Henize, G. 1967, Ap. J. 150, 835.

Reay, N. K. and Ring, J. 1969, Planet. Space Sci., 17, 561.

Reynolds, R. J., Roesler, F. L., Scherb, F., and Boldt, E. 1971, The Gum Nebula and Related Problems (Proceedings of a Conference at Goddard Space Flight Center, Preliminary Edition), pp. 182-209.

Schmitter, E. F. 1971, A. J., 76, 571.

Silk, J. and Werner, M. W. 1969, Ap. J. 158, 185.

Tinsley, B. A. 1970, Space Res., 10, 582.

Walmsley, M. and Grewing, M. 1971, Astrophys. Let. 9, 185.

FIGURE CAPTIONS

Figure 1. H-beta scans in the direction: $l^{II} = 184.5^{o}$, $b^{II} = -5.8^{o}$. (a) Sum of scans made on 1971 October 14-15 and 1971 October 26-27. (b) Sum of scans made on 1972 January 19-20. The LSR and the position and FWHM of the neutral galactic hydrogen as measured by 21-cm radiation are indicated on each graph.

Figure 2. H-alpha scans in the direction: $l^{II} = 184.5^{o}$, $b^{II} = -5.8^{o}$. (a) Sum of scans made on 1972 January 19-20. (b) Single scan made on 1972 February 14-15. The galactic Hα line in both cases has been nearly obscured by an OH airglow line which, due to the etalon transmission curve, appears at nearly the same velocity as the galactic hydrogen line.

Figure 3. Non-galactic emission. The Hα and Hβ count rates above background at the line center vs. the angle θ between the observation direction and the sun. A rate of 1/sec corresponds to an intensity of approximately 0.5R for Hβ and 1.0R for Hα.

Figure 4. (a) Sum of Hβ scans in the direction: $l^{II} = 170^{o}$, $b^{II} = +23^{o}$. (b) An H-alpha scan in the direction: $l^{II} = 253^{o}$, $b^{II} = +86.5^{o}$. The LSR and the position and FWHM of the neutral galactic hydrogen as measured by 21-cm radiation are indicated on each graph.

Figure 5. Galactic anticenter region. Open circles, observation direction; crosses, positions of bright stars in the Orion constellation and Pleiades cluster; cross-hatched regions, bright HII regions; solid lines, brightness contours around the brighter regions of diffuse galactic emission. Contour values are counts per second above background at line center. A rate of $1s^{-1}$ corresponds to an intensity of approximately 0.8R Hβ.

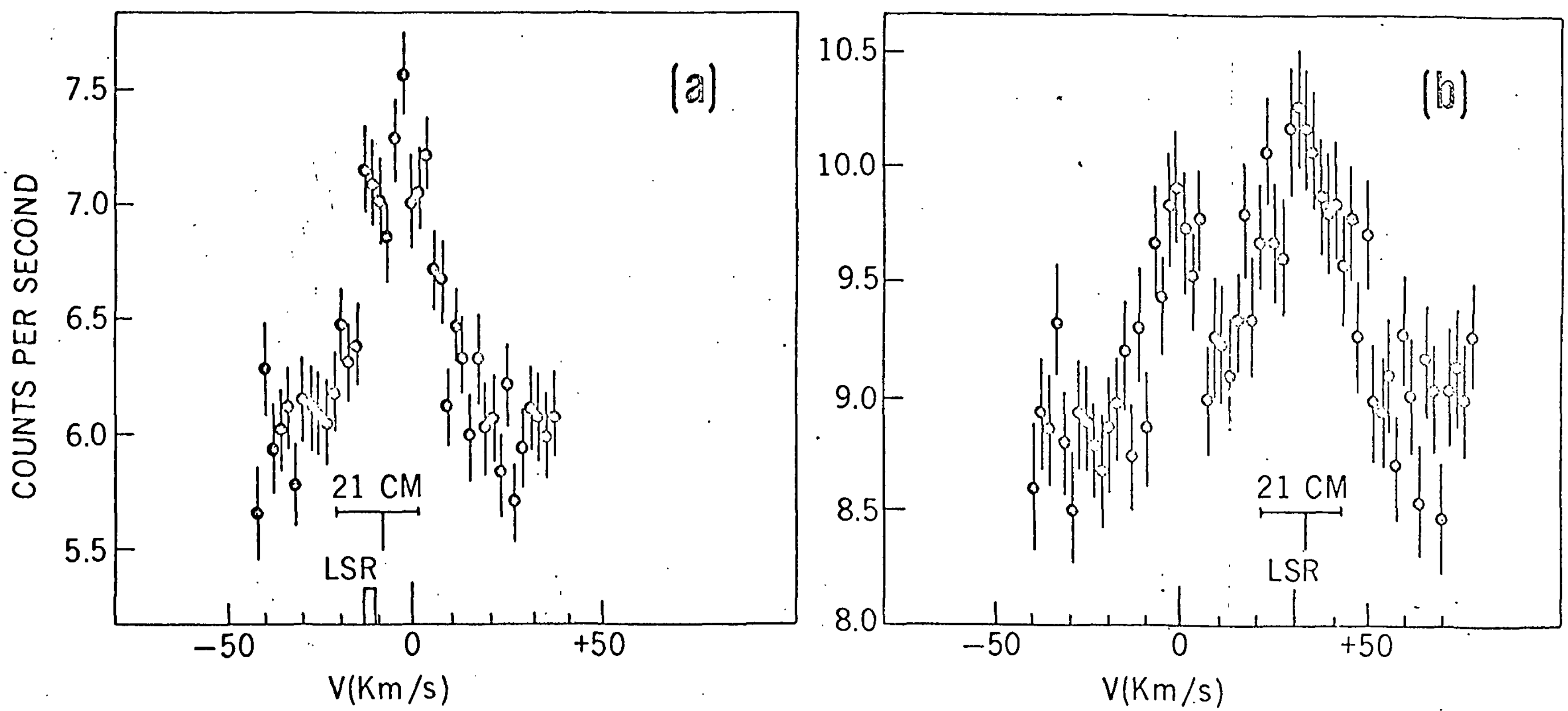
COUNTS PER SECOND
7.5
7.0
6.5
6.0
5.5
(a)
21 CM
LSR
−50
0
+50
V(Km/s)
10.5
10.0
9.5
9.0
8.5
8.0
(b)
21 CM
LSR
−50
0
+50
V(Km/s)

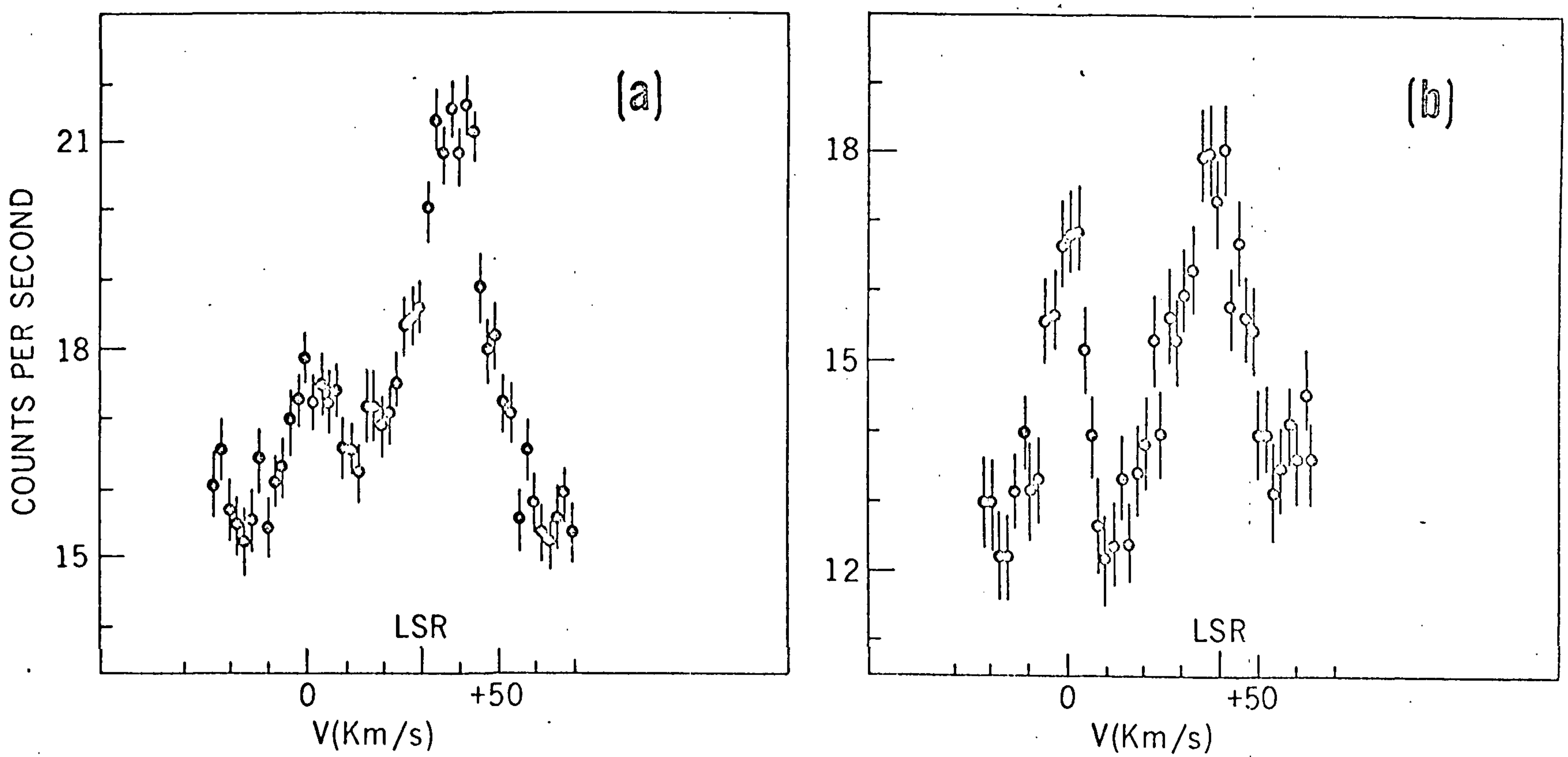
COUNTS PER SECOND
21
18
15
(a)
LSR
0
+50
V(Km/s)
18
15
12
(b)
LSR
0
+50
V(Km/s)

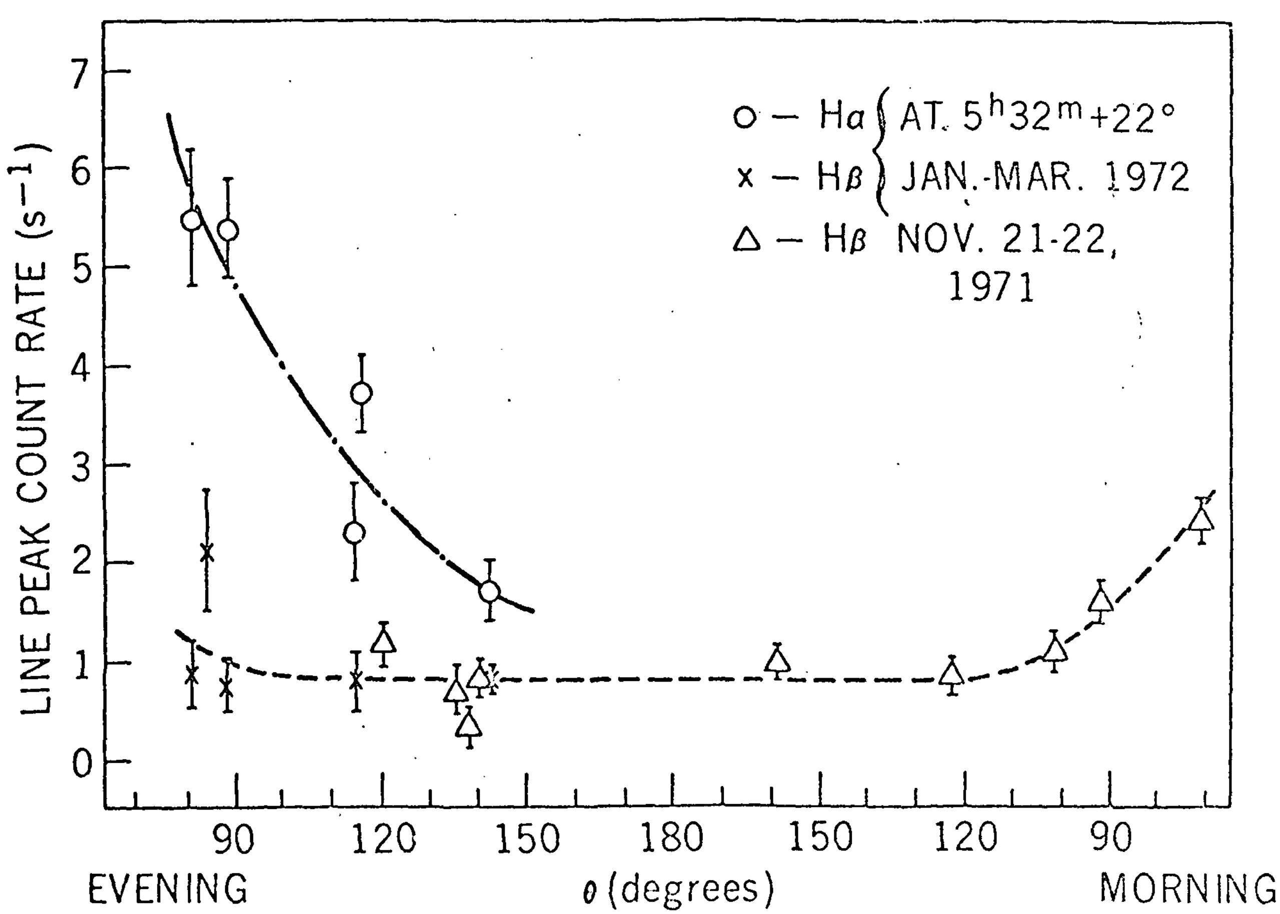
LINE PEAK COUNT RATE (s^{-1})
0
1
2
3
4
5
6
7
○ – Hα AT. 5^h32^m+22°
x – Hβ JAN.-MAR. 1972
△ – Hβ NOV. 21-22, 1971
90
120
150
180
150
120
90
EVENING
θ (degrees)
MORNING

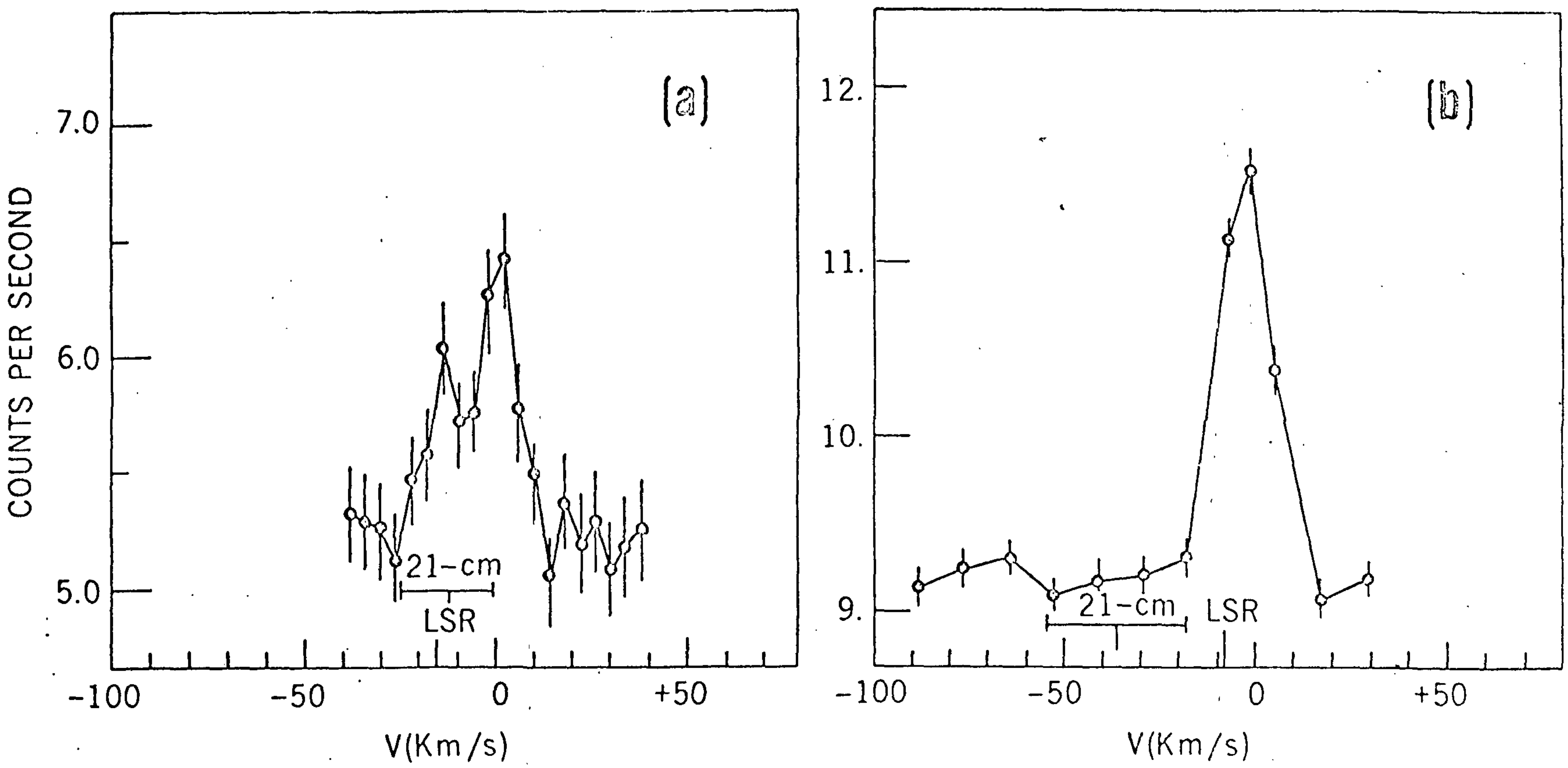
COUNTS PER SECOND
7.0
6.0
5.0
(a)
21-cm
LSR
-100
-50
0
+50
V(Km/s)
12.
11.
10.
9.
(b)
21-cm
LSR
-100
-50
0
+50
V(Km/s)

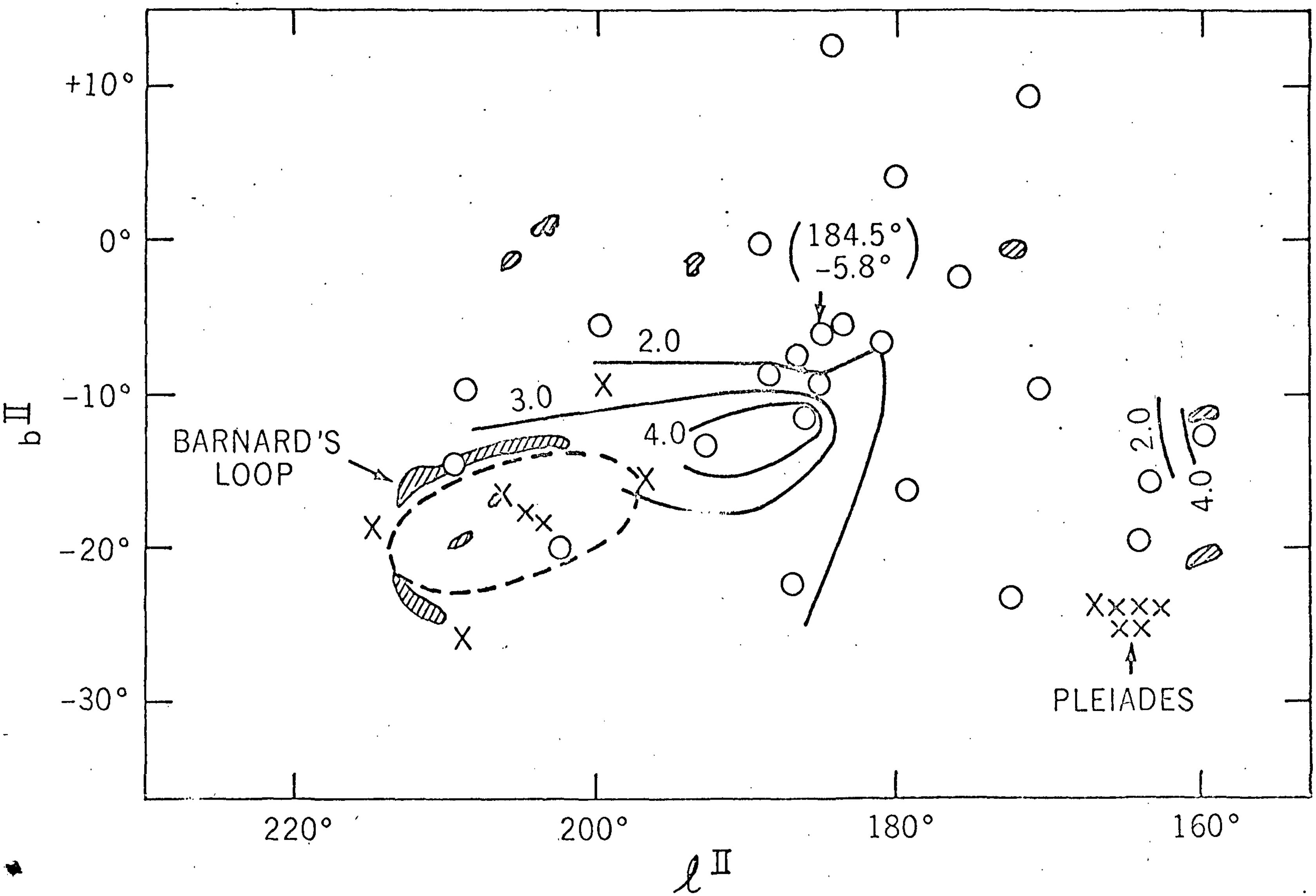

+10°
0°
-10°
-20°
-30°
b^{II}
184.5°
-5.8°
2.0
3.0
4.0
BARNARD'S
LOOP
2.0
4.0
PLEIADES
220°
200°
180°
160°
ℓ^{II}